

# Neutrino Physics

*I. Gil-Botella*

Centro de Investigaciones Energéticas, Medioambientales y Tecnológicas, Madrid, Spain

## Abstract

The fundamental properties of neutrinos are reviewed in these lectures. The first part is focused on the basic characteristics of neutrinos in the Standard Model and how neutrinos are detected. Neutrino masses and oscillations are introduced and a summary of the most important experimental results on neutrino oscillations to date is provided. Then, present and future experimental proposals are discussed, including new precision reactor and accelerator experiments. Finally, different approaches for measuring the neutrino mass and the nature (Majorana or Dirac) of neutrinos are reviewed. The detection of neutrinos from supernovae explosions and the information that this measurement can provide are also summarized at the end.

## 1 Introduction

The last 20 years have been a revolution for neutrino physics. The observation of neutrino oscillations has established that neutrinos have masses and this implies physics beyond the Standard Model. This fact has a clear impact not only on particle physics, but also on astroparticle physics and cosmology.

Nevertheless, neutrinos are still quite unknown particles. At the moment we know that there are three light neutrinos, although some theoretical models propose the existence of sterile neutrinos (not interacting weakly with matter). Neutrinos are much lighter than their charged leptonic partners and they interact very weakly with matter. In addition, during the last 13 years, neutrino experiments have proved that neutrinos have mass, contrary to the zero-neutrino-mass hypothesis of the Standard Model. Neutrinos oscillate when they propagate through space. During the past few years the solar neutrino problem has been solved and the solar and atmospheric oscillation parameters have been confirmed using artificial sources. A period of precision measurements in neutrino physics has started.

However, many fundamental questions still remain unanswered: What is the value of the neutrino masses? Are neutrinos Majorana or Dirac particles? What is the mass hierarchy? What is the value of the neutrino oscillation parameters, in particular,  $\theta_{13}$  and  $\theta_{23}$  (if this is maximal or not)? Is there CP-violation in the leptonic sector? Are there more than three neutrinos? What is the relation with the quark sector? Can neutrinos be related to leptogenesis? Why are neutrinos much lighter than other fermions? ... In summary, there are many aspects of neutrinos still unknown.

The history of neutrinos began with the investigation of beta decays. During the early decades of the past century, radioactivity was explored and the nuclear beta decay was observed. In this process, a radioactive nucleus emits an electron and increases its positive charge by one unit to become the nucleus of another element. The beta decay was studied and, because of the energy conservation, the electron should always carry away the same amount of energy. A line in the energy spectrum was expected.

However, in 1914, Chadwick showed that electrons follow a continuous spectrum of energies up to the expected value. Some of the energy released in the decay appeared to be lost. To explain this observation, only two solutions seemed possible: either energy is not conserved (preference of Bohr) or an additional undetectable particle carrying away the additional energy was emitted (preference of Pauli). To solve the energy crisis, in 1930 Pauli wrote his famous letter explaining that he invented a desperate remedy to save the energy conservation law. There could exist in the nuclei electrically neutral particles that were emitted in beta decays and able to cross the detectors without leaving any trace. These particles (which he wished to call neutrons) were carrying all the missing energy. These particles have spin 1/2 and obey the exclusion principle. The mass should be the same order of magnitude as the electron mass.

Later on, in 1932, Chadwick discovered the neutron; and, in 1934, Fermi took Pauli's idea and on its basis developed a theory of beta decay. Fermi named this particle "neutrino". The weak force is so weak that the probability of inverse beta decay was calculated to be close to zero. The possibility to detect a neutrino seemed null.

However, the development of very intense sources of neutrinos (fission bombs and fission reactors) changed the prospect. In 1951, Reines thought about using an intense burst of antineutrinos from bombs in an experiment designed to detect them. At the end, they decided to use fission reactors as sources, in particular the Hanford reactor. In collaboration with Cowan at the Los Alamos Scientific Laboratory, they began the "Poltergeist Project". They chose the inverse beta decay on protons to detect the free neutrino. The detection principle was a coincident measurement of the 511 keV photons associated with positron annihilation and a neutron capture reaction a few microseconds later. The idea was to build a large detector filled with liquid scintillator loaded with Cd to increase the probability of capturing a neutron. The process releases 9 MeV gammas a few microseconds later than the positron detection. This delayed coincidence provides a powerful means to discriminate the signature of the inverse beta decay from background noise. The 300 litre neutrino detector was read by 90 two-inch photomultipliers (PMTs) and surrounded by homemade boron-paraffin shielding intermixed with lead to stop reactor neutrons and gamma rays from entering the detector and producing unwanted background. The expected rate for delayed coincidences from neutrino-induced events was 0.1–0.3 counts per minute. However, the delayed-coincidence background, present whether or not the reactor was on, was about 5 counts per minute, many times higher than the expected signal rate. The background was due to cosmic rays entering the detector. The small increase observed when the reactor was on was not sufficient. The results of this first experiment were not conclusive.

Nevertheless, after the unsuccessful trial, they redesigned the experiment to better distinguish events induced by cosmic rays and those initiated by reactor neutrinos. Two large flat plastic target tanks were filled with water. The protons in the water provided the target for inverse beta decay. Cadmium chloride dissolved in the water provided the Cd nuclei that would capture the neutrons. The target tanks were sandwiched between three large scintillator detectors having 110 PMTs to collect scintillation light and produce electronic signals. With this detector, neutrinos were detected for the first time in 1956 by Reines and Cowan using the nuclear reactor neutrinos from the Savannah River Plant in South Carolina [1]. Several tests confirmed that the signal was due to reactor antineutrinos. The experiment was also able to provide a measurement of the cross-section for inverse beta decay. This detection was rewarded with the Nobel Prize in 1995.

Other important historical facts related to neutrinos were the detection of muon neutrinos in 1962, the detection of solar neutrinos by Davis in 1970, the discovery of neutral current neutrino interactions in 1973 with a bubble chamber experiment in a  $\nu_\mu$  beam at CERN, the detection of neutrinos from a supernova type-II explosion in 1987 with large underground neutrino detectors, and the determination at the Large Electron-Positron Collider (LEP) of three light neutrinos by measuring the total decay width of the Z resonance.

## 2 Neutrinos in the Standard Model

In the Standard Model (SM) of particle physics, fermions come in three families. Among them, neutrinos are the less known particles. We know that they have zero electric charge and they only interact via weak interactions.

The SM is based on the gauge group  $SU(3)_C \times SU(2)_L \times U(1)_Y$  that is spontaneously broken to the subgroup  $SU(3)_C \times U(1)_{EM}$ . All the fermions of the SM are representations of this group with the quantum numbers indicated in Table 1, where the family structure is shown. Neutrinos are the partners of the charged leptons. They form left-handed weak isospin doublets under the  $SU(2)$  gauge symmetry. In the SM, neutrinos are strictly massless. They do not carry electromagnetic or colour charge but only

the weak charge. They are extremely weakly interacting.

**Table 1:** Fermionic representations in the Standard Model.

$L_L(1, 2, -\frac{1}{2})$	$Q_L(3, 2, \frac{1}{6})$	$E_R(1, 1, -1)$	$U_R(3, 1, \frac{2}{3})$	$D_R(3, 1, -\frac{1}{3})$
$\begin{pmatrix} \nu_e \\ e \end{pmatrix}_L$	$\begin{pmatrix} u \\ d \end{pmatrix}_L$	$e_R$	$u_R$	$d_R$
$\begin{pmatrix} \nu_\mu \\ \mu \end{pmatrix}_L$	$\begin{pmatrix} c \\ s \end{pmatrix}_L$	$\mu_R$	$c_R$	$s_R$
$\begin{pmatrix} \nu_\tau \\ \tau \end{pmatrix}_L$	$\begin{pmatrix} t \\ b \end{pmatrix}_L$	$\tau_R$	$t_R$	$b_R$

Under charge, parity and time reversal symmetry (CPT) conservation, for any left-handed fermion there exists a right-handed antiparticle with opposite charge. But the right-handed particle state may not exist. This is precisely what happens with neutrinos in the SM. Since, when the SM was postulated, neutrino masses were compatible with zero, neutrinos were postulated to be Weyl fermions: the left-handed particle was the neutrino and the right-handed antiparticle was the antineutrino.

A neutrino of a flavour  $l$  is defined by the charged-current (CC) interaction with the corresponding charged lepton  $l$ . For example, the muon neutrino always comes with the charged muon. The CC interactions between neutrinos and their corresponding charged leptons are given by

$$-\mathcal{L}_{CC} = \frac{g}{\sqrt{2}} \sum_l \bar{\nu}_{Ll} \gamma^\mu l_L W_\mu^+ + \text{h.c.} \quad (1)$$

The SM neutrinos also have neutral-current (NC) interactions, as indicated in

$$-\mathcal{L}_{NC} = \frac{g}{2 \cos \theta_W} \sum_l \bar{\nu}_{Ll} \gamma^\mu \nu_{Ll} Z_\mu^0. \quad (2)$$

From this equation, one can determine the decay width of the  $Z^0$  boson into neutrinos, which is proportional to the number of light left-handed neutrinos.

We know thanks to neutrinos that there are exactly three families in the SM. An extra SM family with quarks and charged leptons so heavy that they remain unobserved would also have massless neutrinos that would have been produced in Z decay, modifying its width, which has been measured at LEP with impressive precision. The combined result from the four LEP experiments is  $N_\nu = 2.984 \pm 0.008$  [2].

The SM presents an accidental global symmetry. This is a consequence of the gauge symmetry and the representations of the physical states. The total lepton number given by  $L = L_e + L_\mu + L_\tau$  is conserved.

Other neutrino properties summarized in the Particle Data Book [2] are upper limits on neutrino masses, on neutrino decay processes and on the neutrino magnetic moment.

### 3 Neutrino interactions and detection

Neutrinos are produced copiously in natural sources: in the burning of stars, in the interaction of cosmic rays, in the Earth's radioactivity, in supernova explosions and even as relics of the Big Bang. In the laboratory, neutrinos are produced in nuclear reactors and particle accelerators.

The neutrino energies expand through a huge range: from  $10^3$  eV to  $10^{15}$  eV. In the low-energy range there are neutrinos from double-beta decay, geoneutrinos, nuclear reactors, supernovas and the Sun. Artificial neutrinos from particle accelerators, beta beams or neutrino factories have energies in the medium range. Atmospheric neutrinos extend from medium to high energies, while neutrinos coming from extragalactic sources can reach very high energies.

Another important ingredient for neutrino detection is the neutrino interaction cross-section. Neutrino cross-sections are not equally well known in the whole range (Fig. 1). For neutrino energies lower than 100 MeV, cross-sections are well known because the interaction processes are dominated by the inverse beta decay, elastic scattering, and CC and NC interactions with nuclei. These interactions are theoretically better known than determined in experiments. For neutrino energies above 100 GeV, up to  $10^7$  GeV (ultrahigh energies), they are also accurately known. However, in the intermediate range, critical for atmospheric and accelerator experiments with neutrino energies around 1 GeV, cross-sections are poorly known (with uncertainties of 20–40%) due to the complexity of the processes like quasi-elastic (QE) scattering, single pion production, deep inelastic scattering (DIS), and nuclear effects, form factors, etc.

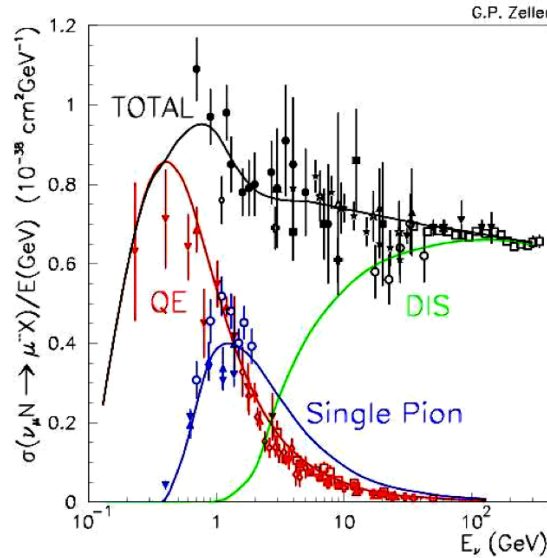


**Fig. 1:** Neutrino interaction cross-sections.

MINER $\nu$ A [3] (Main Injector Experiment for  $\nu$ -A) is a detector designed to precisely study neutrino–nucleus interactions in the 1–10 GeV range in the NuMI high-intensity neutrino beam at Fermilab. This experiment will improve our knowledge of neutrino cross-sections at low energy and study the  $A$  dependence in neutrino interactions. These data will be important to reduce the systematic errors in long-baseline neutrino oscillation experiments.

They will study four main reaction channels: QE, resonance production, deep inelastic scattering, and coherent neutrino–nucleus reactions (CC and NC coherent single pion production). The MINER $\nu$ A detector is a fine-grained tracking calorimeter with a fully active solid-scintillator tracker. The active detector are solid-scintillator strips of triangular cross-section providing a spatial resolution of 2.5 mm. The scintillation light due to a charged particle is collected by a wavelength-shifting optical fibre located at the centre of each strip and routed to PMTs. The detectors are hexagonal modules containing one or two active planes. After the tracker region there is the electromagnetic calorimeter (ECAL) and the hadronic calorimeter (HCAL) to contain forward-going particles. Both calorimeters also surround the inner detector to contain particles with high transverse momentum. At the back of the detector they use

the MINOS Near detector as a muon spectrometer to measure the energy and charge of muons. Before the tracker there is an area of the nuclear targets (liquid He, carbon, iron, lead and water) interleaved with tracking planes. Just before, there is a veto wall and a steel shield.

The MINER $\nu$ A collaboration built a first prototype of 24 full-size modules that was first commissioned with cosmic rays in 2008–2009 and then moved underground into the NuMI beam upstream of the MINOS Near detector with an iron target prototype and a veto wall. It began operating in summer 2009. The complete detector was finished in March 2010. Modules of four types (120 in total) – nuclear target, tracker, ECAL and HCAL – were built with a total mass of  $\sim 200$  ton. MINER $\nu$ A has taken data in the low-energy (peak at 3 GeV) antineutrino beam since November 2009 with 55% of the full detector. In March 2010 they took data in low-energy neutrino mode until September 2010. After November 2010 they took antineutrino data, turning again to low-energy neutrino mode in spring 2011. In summer 2012 Fermilab will switch to the medium-energy beam (peak at 6 GeV) for NO $\nu$ A, and MINER $\nu$ A will continue to take data.

Different technologies have been used by past and present neutrino detectors. *Radiochemical techniques* were used by the first solar neutrino experiments like Homestake, SAGE and GALLEX. They use the interaction of neutrinos with Cl or Ga isotopes, producing Ar or Ge, and developed methods to extract these isotopes using different solutions. They were not real-time detectors. At present, one of the most common technologies exploited is that used by *Cerenkov detectors* like Super-Kamiokande, SNO, MiniBooNE, Antares, IceCube, etc. They detect the Cerenkov light of the charged leptons produced by neutrinos using PMTs. The pattern of the detected rings allows electrons to be distinguished from muons. This is the best technique for low rates and low-multiplicity events with energies below 1 GeV and also very high energies. A different technique used by some neutrino accelerator experiments like MINOS, MINER $\nu$ A and NO $\nu$ A is *tracking calorimetry*. They use alternating planes of absorber material (such as lead) with detector planes for tracking (essentially liquid or plastic scintillators read by PMTs). This is appropriate for high-rate and high-multiplicity events with energies around 1 GeV. Another type of detectors are the *unsegmented scintillator calorimeters* like KamLAND, Borexino and Double Chooz. They provide large light yields at MeV energies. This is very convenient for the detection of reactor and solar neutrinos. *Liquid argon time projection chambers* (LAr TPCs) like ICARUS have high granularity and are potentially good for large masses. Finally we have the *emulsion technique*, which is in fashion again with the OPERA experiment. This is the only technique providing the micrometre-level spatial resolution needed, for example, to detect tau neutrinos.

#### 4 Massive neutrinos

As already mentioned, there are only upper limits to neutrino masses. The direct limits come from the precise measurement of the endpoint of the lepton energy spectrum in weak decays, which gets modified if neutrinos are massive.

The SM predicts that neutrinos are precisely massless. In order to add a mass to the neutrino, the SM has to be extended. The SM gauge invariance does not imply lepton number symmetry. Total lepton number can or cannot be a symmetry depending on the neutrino nature.

Neutrino masses can be easily accommodated in the SM. A massive fermion necessarily has two states of helicity. The mass is the strength of the coupling between the two helicity states. To introduce such a coupling in the SM for the neutrinos, we need to identify the neutrino right-handed states, which in the SM are absent. There are two ways to proceed:

1. We introduce a right-handed neutrino coupled to the matter just through the neutrino masses and impose lepton number conservation (*Dirac neutrinos*)

$$\mathcal{L} = \mathcal{L}_{\text{SM}} - M_\nu \bar{\nu}_R \nu_L + \text{h.c.} \quad (3)$$

2. We do not impose lepton number conservation and we identify the right-handed state with the antiparticle of the left-handed state (*Majorana neutrinos*)

$$\mathcal{L} = \mathcal{L}_{\text{SM}} - \frac{1}{2} M_\nu \overline{\nu_L^C} \nu_L + \text{h.c.} \quad (4)$$

In the first case, we enlarge the SM by adding a set of three right-handed neutrino states, which would be singlets under  $SU(3) \times SU(2) \times U_Y(1)$ , but coupled to matter just through the neutrino masses. This coupling has to be of the Yukawa type to preserve the gauge symmetry. Masses are proportional to the vacuum expectation value of the Higgs field, like for the remaining fermions. One important consequence of this is a new hierarchical problem: Why are neutrinos much lighter than the remaining leptons?

In the second case, Majorana identified the right-handed state with the antiparticle of the left-handed state.  $C$  is the operator of charge conjugation in spinor space that connects particle and antiparticles:

$$\nu_R \rightarrow (\nu_L)^c = C \overline{\nu_L^T} = C \gamma_0 \nu_L^* \quad (5)$$

The Majorana neutrino masses are of the form

$$m_\nu = \alpha_\nu \frac{v^2}{\Lambda}. \quad (6)$$

If  $\Lambda$  is much higher than the electroweak scale  $v$ , a strong hierarchy between neutrino and charged lepton masses arises naturally. A Majorana mass violates the conservation of all charges carried by the fermion, including global charges as lepton number.

The simplest example to explain the origin of the scale  $\Lambda$  in the Majorana masses is the famous *see-saw mechanism* [4]. In this case, the scale of the mass eigenvalues is much higher than the scale of electroweak symmetry breaking ( $\Lambda \gg v$ ). The Majorana effective interaction results from the interchange of very heavy right-handed Majorana neutrinos. The new physics scale is simply related to the masses of the heavy Majorana neutrinos and the Yukawa couplings.

Neutrino masses imply neutrino mixing, as happens in the quark sector. Majorana and Dirac possibilities differ in the number of observable phases. The real physical parameters are the mass eigenstates and the mixing angles, while the imaginary parameters are CP-violating phases. In the case of three families, there are three mixing angles and one phase for the Dirac case or three phases for the Majorana case.

## 5 Neutrino oscillations in vacuum and matter

If neutrinos have masses and mix, there can be neutrino flavour change. Oscillations appear because of the misalignment between the neutrino interaction eigenstates and the propagation mass eigenstates.

The neutrino flavour eigenstates,  $\nu_\alpha$ , produced in a weak interaction are linear combinations of the mass eigenstates  $\nu_j$ :

$$|\nu_\alpha\rangle = \sum_{j=1}^n U_{\alpha j}^* |\nu_j\rangle, \quad (7)$$

where  $n$  is the number of light neutrino species and  $U$  is the Pontecorvo–Maki–Nakagawa–Sakata (PMNS) mixing matrix.

A standard parametrization of the mixing matrix is given by

$$U_{\text{PMNS}} = \begin{pmatrix} 1 & 0 & 0 \\ 0 & c_{23} & s_{23} \\ 0 & -s_{23} & c_{23} \end{pmatrix} \begin{pmatrix} c_{13} & 0 & s_{13} e^{i\delta} \\ 0 & 1 & 0 \\ -s_{13} e^{i\delta} & 0 & c_{13} \end{pmatrix} \begin{pmatrix} c_{12} & s_{12} & 0 \\ -s_{12} & c_{12} & 0 \\ 0 & 0 & 1 \end{pmatrix} \begin{pmatrix} 1 & 0 & 0 \\ 0 & e^{i\alpha_1} & 0 \\ 0 & 0 & e^{i\alpha_2} \end{pmatrix}, \quad (8)$$

where  $c_{ij} = \cos \theta_{ij}$  and  $s_{ij} = \sin \theta_{ij}$ , with  $\theta_{12}$ ,  $\theta_{13}$  and  $\theta_{23}$  the three mixing angles,  $\delta$  is the Dirac CP-violating phase, and  $\alpha_1$  and  $\alpha_2$  are the Majorana phases, not accessible by oscillation experiments.

After travelling a distance  $L$  (or, equivalently for relativistic neutrinos, time  $t$ ), a neutrino originally produced with a flavour  $\alpha$  evolves as follows:

$$|\nu_\alpha(t)\rangle = \sum_{j=1}^n U_{\alpha j}^* |\nu_j(t)\rangle. \quad (9)$$

Using the standard approximation that the neutrino state is a plane wave  $|\nu_j(t)\rangle = e^{-iE_j t} |\nu_j(0)\rangle$ , that neutrinos are relativistic with

$$E_j = \sqrt{p_j^2 + m_j^2} \approx p + \frac{m_j^2}{2E} \quad (10)$$

and the orthogonality relation  $\langle \nu_i(0) | \nu_j(0) \rangle = \delta_{ij}$ , the transition probability between  $\nu_\alpha$  and  $\nu_\beta$  is

$$\begin{aligned} P(\nu_\alpha \rightarrow \nu_\beta) &= |\langle \nu_\beta | \nu_\alpha(t) \rangle|^2 = \left| \sum_{j=1}^n \sum_{k=1}^n U_{\alpha j}^* U_{\beta k} \langle \nu_k | \nu_j(t) \rangle \right|^2 \\ &\approx \sum_{j,k} U_{\alpha j}^* U_{\beta j} U_{\alpha k} U_{\beta k}^* e^{-i\Delta m_{jk}^2 L/2E}, \end{aligned} \quad (11)$$

with  $\Delta m_{jk}^2 = m_j^2 - m_k^2$ . The probability for flavour transition is a periodic function of the distance between the source and the detector.

Dominant oscillations are well described by effective two-flavour oscillations. The three-flavour oscillation neutrino effects are suppressed because of the small value of  $\theta_{13}$  and the hierarchy between the two mass splittings,  $\Delta m_{21}^2 \ll \Delta m_{32}^2$ . In most cases the problem can be reduced to two-flavour oscillations.

In the simplest case of two-family mixing, the mixing matrix depends on just one mixing angle and there is only one mass square difference. The probability that a neutrino  $\nu_\alpha$  of energy  $E_\nu$  oscillates into a neutrino  $\nu_\beta$  after travelling a distance  $L$  is given by

$$P(\nu_\alpha \rightarrow \nu_\beta) = \sin^2 2\theta \sin^2 \left( \frac{\Delta m^2 L}{4E_\nu} \right), \quad \alpha \neq \beta. \quad (12)$$

The probability is the same for neutrinos and antineutrinos, since there are no imaginary entries in the mixing matrix.

The transition probability has an oscillatory behaviour with a period determined by the oscillation length ( $L_{\text{osc}}$ ), which is proportional to the neutrino energy and inversely proportional to the neutrino mass square difference, and an amplitude proportional to the mixing angle. Hence the name ‘‘neutrino oscillations’’:

$$L_{\text{osc}} = \frac{4\pi E_\nu}{\Delta m^2}. \quad (13)$$

If  $L \gg L_{\text{osc}}$ , the oscillating phase goes through many cycles before detection and is averaged to 1/2.

Experimentally, the free parameters are the source–detector distance and the neutrino energy. In order to be sensitive to a given value of  $\Delta m^2$ , the experiment has to be set up with  $E/L \approx \Delta m^2$ . For example, to measure  $\theta_{23}$  and  $\Delta m_{32}^2$  parameters, one should look for an  $L/E$  of around 500 km/GeV (which is the case for atmospheric neutrinos). To measure  $\theta_{12}$  and  $\Delta m_{21}^2$  parameters  $L/E$  should be around 15 000 km/GeV (solar neutrinos case).

In the most general case of three neutrino families, the oscillation probability can be rewritten in one term conserving CP and another term violating CP, as follows:

$$P(\nu_\alpha \rightarrow \nu_\beta) = \delta_{\alpha\beta} - 4 \sum_{i < j}^n \text{Re}[J_{ij}^{\alpha\beta}] \sin^2 \left( \frac{\Delta m_{ij}^2 L}{4E_\nu} \right) \pm 2 \sum_{i < j}^n \text{Im}[J_{ij}^{\alpha\beta}] \sin \left( \frac{\Delta m_{ij}^2 L}{2E_\nu} \right), \quad (14)$$

with  $J_{ij}^{\alpha\beta} \equiv U_{\alpha i} U_{\beta i}^* U_{\alpha j}^* U_{\beta j}$ . The two terms have opposite sign for neutrinos and antineutrinos. By comparing neutrino and antineutrino oscillation probabilities, we could test the violation of CP.

From the experimental point of view, to measure neutrino oscillations, we need to compute or to measure the flavour composition and the flux and energy spectra of the produced neutrinos (near data) and also the interaction cross-section at their energies. After propagation of neutrinos through a distance  $L$ , we need to measure the flavour composition and energy spectrum (far data) with a detector. By comparing predictions with observations or near/far data, we can measure neutrino oscillations and determine the oscillation parameters.

When neutrinos propagate in matter, the interactions with the medium affect their properties. The amplitude of this propagation is modified due to coherent forward scattering on electrons and nucleons. Different flavours have different interactions. The effect of the medium can be described by an effective potential that depends on the density and composition of the matter.

The effective potential for the evolution of  $\nu_e$  in a medium with electrons, protons and neutrons due to its CC interactions is given by

$$V_{\text{CC}} = \pm \sqrt{2} G_F n_e, \quad (15)$$

where  $n_e$  is the electron number density and  $G_F$  is the Fermi constant. The effective potential has different sign for neutrinos and antineutrinos.

For example, the matter potential at the Earth's core is  $\sim 10^{-13}$  eV while at the solar core it is  $\sim 10^{-12}$  eV. In spite of these tiny values, these effects are non-negligible in neutrino oscillations.

For  $\nu_\mu$  and  $\nu_\tau$ , the potential due to CC interactions is zero, since neither muons nor taus are present in the medium. The effective potential for any active neutrino due to neutral current interactions in a neutral medium can be written as

$$V_{\text{NC}} = \mp \frac{\sqrt{2}}{2} G_F n_n \quad (16)$$

where  $n_n$  is the number density of neutrons.

In general, the electron number density in the medium changes along the neutrino trajectory and so does the effective potential. We can describe neutrino oscillations in a medium as in vacuum but with an effective mass matrix ( $\tilde{M}_\nu^2$ ) that depends on the neutrino energy and the matter density, as follows:

$$\tilde{M}_\nu^2 = M_\nu^2 \pm 4EV_m, \quad (17)$$

with

$$V_m = \begin{pmatrix} V_e = V_{\text{CC}} + V_{\text{NC}} & 0 & 0 \\ 0 & V_\mu = V_{\text{NC}} & 0 \\ 0 & 0 & V_\tau = V_{\text{NC}} \end{pmatrix}. \quad (18)$$

In the case of two flavours, the mixing angle and effective masses in matter can be written as

$$\tan 2\theta_m = \frac{\Delta m^2 \sin 2\theta}{\Delta m^2 \cos 2\theta - A} \quad (19)$$

and

$$\mu_{1,2}^2(x) = \frac{m_1^2 + m_2^2}{2} + E(V_\alpha + V_\beta) \mp \frac{1}{2} \sqrt{(\Delta m^2 \cos 2\theta - A)^2 + (\Delta m^2 \sin 2\theta)^2}. \quad (20)$$



They depend on the matter density and neutrino energy. The  $- (+)$  sign corresponds to neutrinos (anti-neutrinos). The quantity  $A$  is defined as  $A \equiv 2E(V_\alpha - V_\beta)$ , the potential difference factor between  $\alpha$  and  $\beta$  flavours. Depending on the sign of  $A$ , the mixing angle in matter can be larger or smaller than in vacuum. For constant potential, the mixing angle and effective masses are constant along the neutrino evolution.

Matter effects are important when the potential difference factor  $A$  is comparable to the mass difference term  $\Delta m^2 \cos 2\theta$ . The oscillation amplitude has a resonance when the neutrino energy satisfies this relation:

$$A_R = \Delta m^2 \cos 2\theta. \quad (21)$$

Even if the mixing angle in vacuum is very small, we will have maximal mixing at the resonance condition. The resonance happens for neutrinos or antineutrinos but not for both, and depends on the sign of  $\Delta m^2 \cos 2\theta$ .

The value of the mixing angle in matter changes if the density is changing along the neutrino trajectory. The mixing angle  $\theta_m$  changes sign at  $A_R$ . For  $A \gg A_R$ , we have  $\theta_m = \pi/2$ . For  $A = A_R$ ,  $\theta_m = \pi/4$ .

For a neutrino system that is travelling across a monotonically varying matter potential, the dominant flavour component of a given mass eigenstate changes when crossing the region with  $A = A_R$ . This phenomenon is known as *level crossing*. For constant or sufficiently slowly varying matter potential, the instantaneous mass eigenstates behave approximately as energy eigenstates and they do not mix in the evolution. This is the *adiabatic transition* approximation.

The Mikheyev–Smirnov–Wolfenstein (MSW) effect [5] describes the adiabatic flavour neutrino conversion in a medium with varying density. We can consider the propagation of a two-family neutrino system in the matter density of the Sun. The solar density decreases monotonically with the distance to the centre of the Sun. The eigenstates in matter can be written as

$$|\nu_1^m\rangle = |\nu_e\rangle \cos \theta_m - |\nu_\mu\rangle \sin \theta_m, \quad (22)$$

$$|\nu_2^m\rangle = |\nu_e\rangle \sin \theta_m + |\nu_\mu\rangle \cos \theta_m. \quad (23)$$

Neutrinos are produced close to the centre where the electron density ( $n_e(0)$ ) is very large. The potential is much larger than the resonance potential

$$2E\sqrt{2}G_F n_e(0) \gg \Delta m^2 \cos 2\theta, \quad (24)$$

and therefore the mixing angle in matter is  $\theta_m = \pi/2$ . In this case, the electron neutrino is mostly the second mass eigenstate ( $\nu_e \approx \nu_2^m$ ).

When neutrinos exit the Sun, the matter density falls to zero and the effective mixing angle is the one in vacuum,  $\theta_m = \theta$ . If  $\theta$  is small, the eigenstate  $\nu_2^m$  is mostly  $\nu_\mu$ . There is maximum conversion  $\nu_e \rightarrow \nu_\mu$  if the adiabatic approximation is correct (Fig. 2). This is the MSW effect. There is a level crossing in the absence of mixing. As we will explain later, the deficit of electron neutrinos coming from the Sun has been interpreted in terms of an MSW effect in neutrino propagation in the Sun.

## 6 Experimental results from neutrino oscillation experiments

Over the years, neutrino experiments have provided spectacular evidence for neutrino oscillations. There are essentially three pieces of evidence: one provided by solar and reactor neutrinos, a second by atmospheric and accelerator neutrinos, and a third by the Liquid Scintillator Neutrino Detector (LSND) experiment. They correspond to three values of mass-squared differences of different orders of magnitude. There is no consistent explanation of all three signals based on oscillations among the three known neutrinos, since there are only two independent mass-squared differences.

In the next sections, I will describe these experimental results in detail.

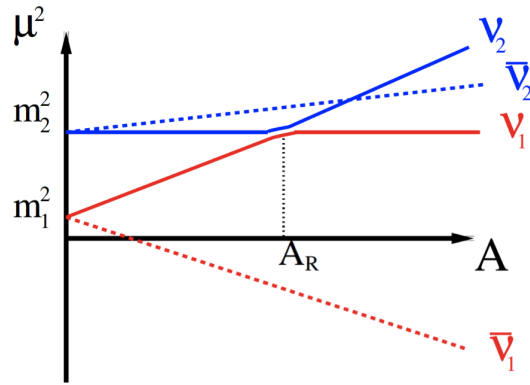


**Fig. 2:** Effective masses acquired in the medium by a system of two massive neutrinos as a function of the potential  $A$ .

### 6.1 Solar neutrinos

Solar electron neutrinos are produced in thermonuclear reactions happening in the Sun through two main chains, the proton–proton (pp) chain and the carbon–nitrogen–oxygen (CNO) cycle. There are five reactions that produce  $\nu_e$  in the pp chain and three in the CNO cycle.

Figure 3 shows the solar neutrino spectrum as predicted by Bahcall [6] from the eight reactions.

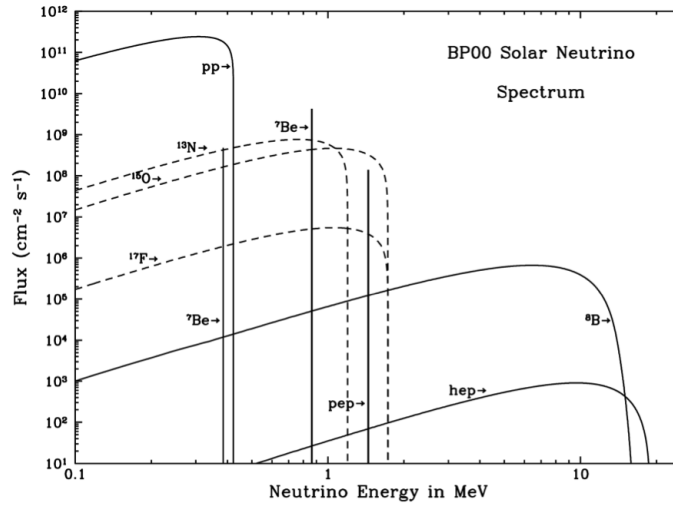


**Fig. 3:** Neutrino fluxes from the pp chain reactions and the CNO cycle reactions as a function of the neutrino energy.

The standard solar model (SSM) is the theoretical model describing the evolution of the Sun and allows one to predict the spectra and the fluxes of all the solar neutrino sources. As a consequence, solar neutrinos provide a unique probe for studying both the nuclear fusion reactions that power the Sun and the fundamental properties of neutrinos.

The first indication of oscillations happened in the 1970s by measuring the solar neutrino flux. Radiochemical experiments were trying to understand the energy production mechanism in the Sun and they found a huge difference between what they measured and what was expected from solar models.

The Davis experiment was installed in the Homestake mine in South Dakota [7]. They built a

615 ton tank of perchloroethylene  $C_2Cl_4$  to measure the  $\nu_e$  interaction with Cl, which gives a radioactive isotope  $^{37}Ar$  that can be extracted and counted.



The energy threshold for this reaction is 0.814 MeV, so the relevant fluxes are the  $^7Be$  and  $^8B$  neutrinos. The  $^{37}Ar$  produced is extracted radiochemically every three months approximately and the number of  $^{37}Ar$  decays is measured in a proportional counter.

In the 1990s, other radiochemical experiments like GALLEX/GNO [8] in Italy and SAGE [9] in Russia tried to measure the solar neutrinos using a  $^{71}Ga$  target and extracting Ge isotopes.



This reaction has a very low energy threshold ( $E_\nu > 0.233$  MeV) and a large cross-section for the lower-energy pp neutrinos. The extraction of  $^{71}Ge$  takes place every 3–4 weeks. The GALLEX programme was completed in the autumn of 1997 and its successor GNO started taking data in spring 1998.

All the radiochemical neutrino experiments found a solar neutrino flux much lower (between 30% and 50%) than the predicted value. They could provide neither information on the directionality nor the energy of the neutrinos.

The Kamiokande experiment [10] pioneered a new technique to observe solar neutrinos using water Cerenkov detectors. This was a real-time experiment and provided information on the directionality and the energy of neutrinos by measuring the electrons scattered from the water by the elastic reaction



producing Cerenkov light, which is detected by photomultipliers. The threshold for this type of experiment is much higher and they are only able to measure the  $^8B$  neutrinos.

Later on, the Super-Kamiokande (SK) experiment [11], with 50 kton of water, measured the solar neutrinos with unprecedented precision in the energy region 5–20 MeV. Figure 4 shows the reconstructed direction of the incoming neutrinos correlated to the Sun direction as measured by SK during the first phase of operation (1996–2001).

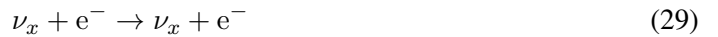
In 2001 the SNO experiment showed clear evidence that solar neutrinos oscillate. This allowed the solar model predictions to be studied independently of the neutrino properties.

SNO [12] is a Cerenkov detector made of 1 kton of heavy water ( $D_2O$ ) located underground in the Sudbury mine in Canada and is able to detect  $^8B$  solar neutrinos via three different reactions:

- CC interactions on deuterons in which only electron neutrinos participate



- elastic scattering (ES) sensitive to other neutrino flavours but dominated by electron neutrinos



- NC interactions with equal sensitivity to all flavours and an energy threshold of 2.2 MeV



In the case of no oscillations, the neutrino fluxes from the three interactions should be equal since there are only electron neutrinos coming from the Sun. However, Fig. 5 shows the neutrino fluxes measured by the three reactions by SNO. The flux of non-electron neutrinos ( $\phi_{\mu\tau}$ ) is plotted as a function of the electron neutrino flux ( $\phi_e$ ). The NC events give a measure of the total solar neutrino flux and it

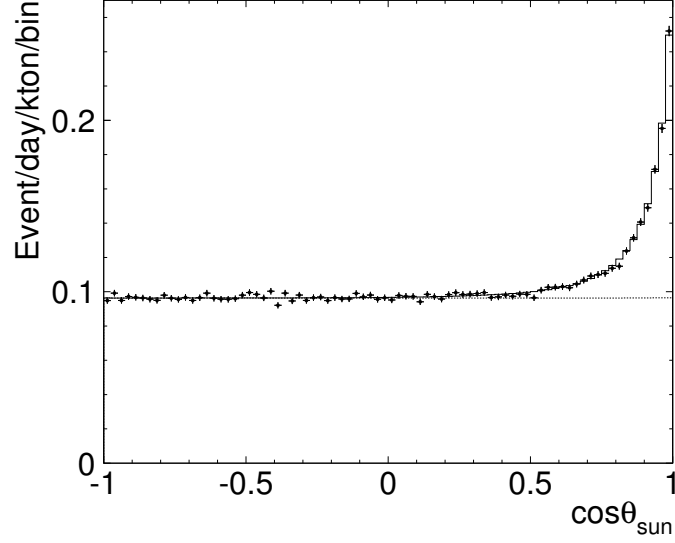


**Fig. 4:** Solar neutrino direction as a function of the zenith angle of the Sun in Super-Kamiokande phase I (from Ref. [11]).

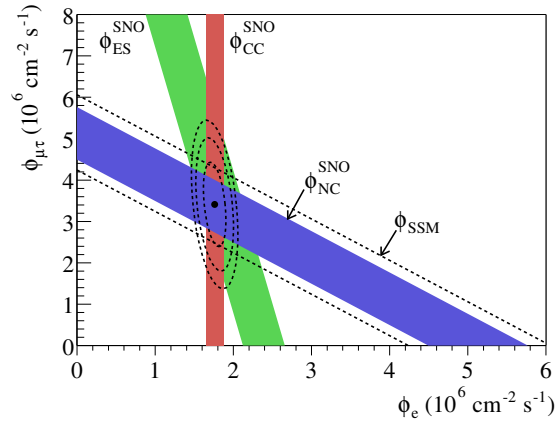


**Fig. 5:** Flux of  $^8\text{B}$  solar neutrinos that are  $\mu$  or  $\tau$  flavour versus flux of electron neutrinos deduced from the three neutrino reactions in SNO (from Ref. [13]).

is in good agreement with the SSM theoretical predictions. SNO can test if the deficit of solar  $\nu_e$  is due to changes in the flavour composition of the solar neutrino beam, since the ratio CC/NC compares the number of  $\nu_e$  interactions with those from all active flavours. This comparison is independent of the overall flux normalization.

The SNO detector operated during 1999–2006 in three phases with different detection techniques to detect NC neutrons: phase I, in pure heavy water; phase II, 2000 kg of salt were dissolved in the heavy water, increasing the neutron capture cross-section; and phase III, the salt was removed and ultra-pure  $^3\text{He}$  counters were deployed into the SNO detector. SNO finished data taking in November 2006.

From the latest results including the SNO-III phase, the ratio between the CC and NC events is [14]

$$\frac{\phi_{CC}}{\phi_{NC}} = 0.301 \pm 0.033. \quad (31)$$

This result provides clear evidence for solar neutrino oscillations independently of the solar model.

From the SNO results, it is possible to constrain the neutrino mixing parameters. Figure 6 shows the allowed regions of parameters from SNO data (left) and from the global analysis including data from all the solar experiments (right). Of all the possible solutions, only the one at the largest mixing angle and mass-squared difference survives, the famous large-mixing-angle (LMA) solution, for which matter effects in the Sun are important.

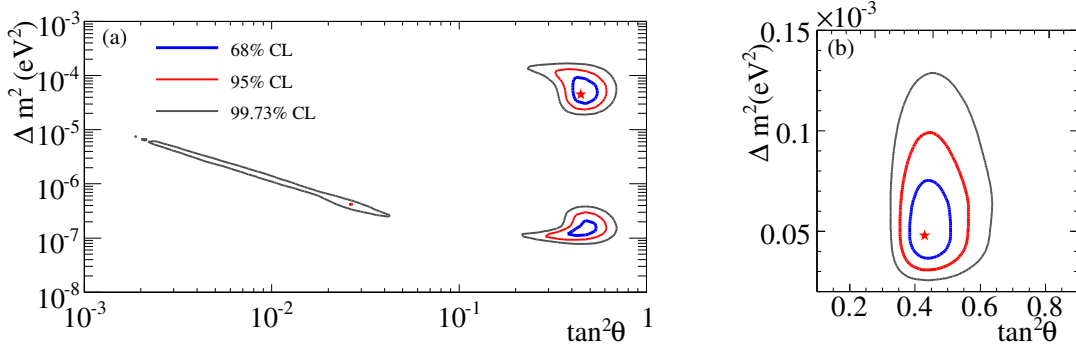


**Fig. 6:** Allowed oscillation parameters from the analysis of SNO neutrino data (left) and from the global analysis of all solar neutrino data (right) in terms of neutrino oscillations (from Ref. [14]).

The phase I and II data from SNO have been reanalysed (see Fig. 7) [15] with a lower effective electron kinetic energy threshold (3.5 MeV). The total uncertainty on the flux of  $^8\text{B}$  solar neutrinos has been reduced by more than a factor of 2 compared to the best previous SNO results.

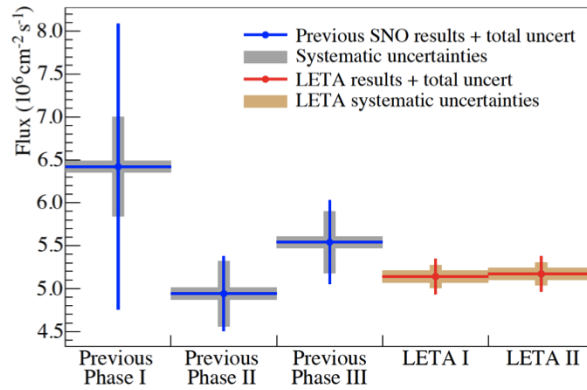


**Fig. 7:** Total  $^8\text{B}$  neutrino flux results using the NC reaction from both unconstrained signal extraction fits (LETA) in comparison to unconstrained fit results from previous SNO analyses (from Ref. [15]).

One of the most important results in the last few years has come from the Borexino detector in the Gran Sasso laboratory. Borexino [16] is a 300 kton ultra-pure liquid scintillator detector using the elastic scattering on electrons to measure the low-energy flux and spectrum of solar neutrinos. The main goal is the measurement of the monochromatic  $^7\text{Be}$  solar neutrinos at 0.862 MeV. Thanks to its excellent radiopurity, Borexino also measures  $^8\text{B}$  neutrinos with an energy threshold of only 3 MeV. This is the lowest energy threshold ever reached in real-time experiments.

Before Borexino, radiochemical experiments measured the very low energy range (where oscillations happen essentially in vacuum) while SNO and SK measured the  $^8\text{B}$  part of the spectrum. Borexino has measured the  $^7\text{Be}$  spectrum and provided a confirmation of the MSW-LMA model. This is the first direct measurement of the survival probability for solar electron neutrinos in the transition region

between matter-enhanced and vacuum-driven oscillations [17].

A prediction of the MSW–LMA model is that neutrino oscillations are dominated by vacuum oscillations at low energies ( $< 1$  MeV) and by resonant matter-enhanced oscillations taking place in the Sun’s core at high energies ( $> 5$  MeV). A measurement of the survival probability as a function of the neutrino energy is very important to confirm the MSW–LMA solution. Figure 8 shows the survival probability ( $P_{ee}$ ) before (left) and after (right) including the Borexino data and the fit assuming LMA oscillations. The MSW–LMA model is confirmed at  $4.2\sigma$  level. For the first time the same apparatus can measure two different oscillation regions predicted by the MSW–LMA model.

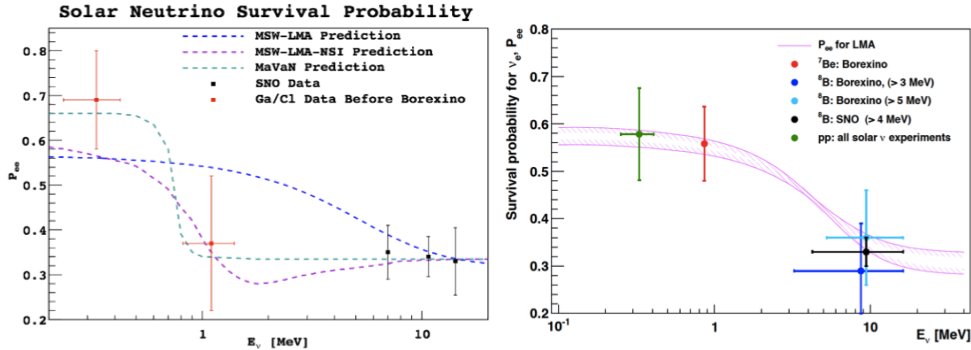


**Fig. 8:** Comparison of solar neutrino fluxes as a function of the energy measured by several solar neutrino experiments before (left) and after (right) Borexino data (from Ref. [18]).

“Geoneutrinos” are electron antineutrinos produced by beta decays of the nuclei in the decay chains of  $^{238}\text{U}$  and  $^{232}\text{Th}$ . Geoneutrinos are direct messengers of the abundances and distribution of radioactive elements within our planet. By measuring their flux and spectrum, it is possible to reveal the distribution of long-lived radioactivity in the Earth and to assess the radiogenic contribution to the total heat balance of the Earth. As these radioactive isotopes beta-decay, they produce antineutrinos. So, measuring these antineutrinos may serve as a cross-check of the radiogenic heat production rate.

KamLAND is the first detector to conduct an investigation on geoneutrinos [19]. In 2005 they provided the first experimental indication for geoneutrinos. Borexino has also been able to measure geoneutrinos at  $4.2\sigma$  [20]. Both detectors use the inverse beta decay to detect geoneutrinos.

## 6.2 Atmospheric neutrinos

Atmospheric neutrinos are produced in the collision of primary cosmic rays (typically protons) with nuclei in the upper atmosphere. This creates a shower of hadrons, mostly pions. The pions decay to a muon and a muon neutrino. The muons decay to an electron, another muon neutrino, and an electron neutrino. Based on this simple kinematic chain, one predicts a flux ratio of two muon neutrinos to one electron neutrino.

The first experiment proving neutrino oscillations without ambiguities was the Super-Kamiokande experiment located 1000 m underground in the Kamioka mine in Japan in 1998. This 50 kton water Cerenkov detector (22.5 kton fiducial mass) measured the atmospheric neutrinos produced by cosmic-ray collisions with the atmosphere. Two muon neutrinos are produced per one electron neutrino from the pion decay with energies between 0.1 and 100 GeV. More than 11 000 20-inch PMTs covering 40% of the surface detect the Cerenkov light coming from the neutrino CC interactions.

By measuring the number of events of each type, as a function of energy and direction, we can find out if neutrino oscillations are affecting the results. SK has shown a big deficit of muon neutrinos dependent on the energy and at distances compatible with neutrino oscillations. The distributions of

electrons and muons as a function of the azimuthal angle show an asymmetry between upward and downward muon neutrinos (Fig. 9). The muon neutrinos traversing the Earth present a clear deficit, which is not the case for downward muon neutrinos or electron neutrinos. This deficit is compatible with a  $\nu_{\mu}-\nu_{\tau}$  oscillation [21].

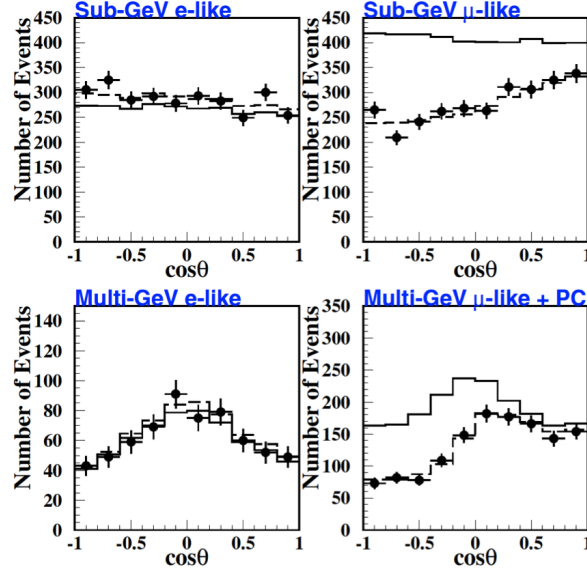


**Fig. 9:** Zenith angle distribution of SK data. Dots, solid line and dashed line correspond to data, Monte Carlo without oscillation, and Monte Carlo with best-fit oscillation parameters.

On 12 November 2001, about 6600 of the photomultiplier tubes in the Super-Kamiokande detector imploded, apparently in a chain reaction due to a shock wave. The detector was partially restored by redistributing the photomultiplier tubes that did not implode. In 2005 they reinstalled 6000 PMTs and they called the new phase SK-III.

The zenith angle two-flavour analysis of the data before the SK PMT implosion (SK-I and SK-II) has been updated [22] and allowed to better constrain the  $\Delta m_{32}^2$  and  $\theta_{23}$  oscillation parameters.

SK was also able to observe the expected dip in the  $L/E$  spectrum due to oscillations (Fig. 10). Other hypotheses have been excluded at  $4.1\sigma$  and  $5\sigma$  levels.

The latest zenith angle and  $L/E$  analysis results from SK-I, II and III data [24] are consistent and provide the most stringent limit on  $\sin^2 \theta_{23}$ .

### 6.3 Reactor neutrinos

Reactor neutrinos have also played a crucial role in neutrino oscillations. They have helped to understand the solar anomaly and they have provided unique information on the  $\theta_{13}$  mixing angle, still unknown.

Nuclear reactors are the major source of human-generated neutrinos. They are very intense, pure and isotropic sources of antineutrinos coming from the beta decay of the neutron-rich fission fragments. The four main isotopes contributing to the antineutrino flux are  $^{235}\text{U}$ ,  $^{238}\text{U}$ ,  $^{239}\text{Pu}$  and  $^{241}\text{Pu}$ .

On average, each fission cycle produces  $\sim 200$  MeV and six antineutrinos. For typical modern commercial light-water reactors with thermal power of the order of 3 GWth, the typical yield is  $\sim 6 \times 10^{20}$  antineutrinos per core per second. But not all these neutrinos can be detected.

The observed neutrino spectrum will be the product of the reactor neutrino flux and the inverse beta decay cross-section, as shown in Fig. 11. The inverse beta decay (Eq. (32)) has an energy threshold

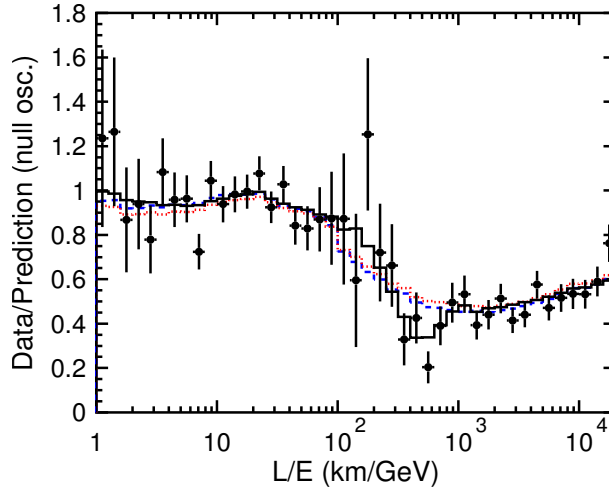


**Fig. 10:** Ratio of the data to the non-oscillated Monte Carlo events (points) with the best-fit expectation for two-flavour  $\nu_\mu \rightarrow \nu_\tau$  oscillation analysis (solid line) as a function of  $L/E$  (from Ref. [23]).

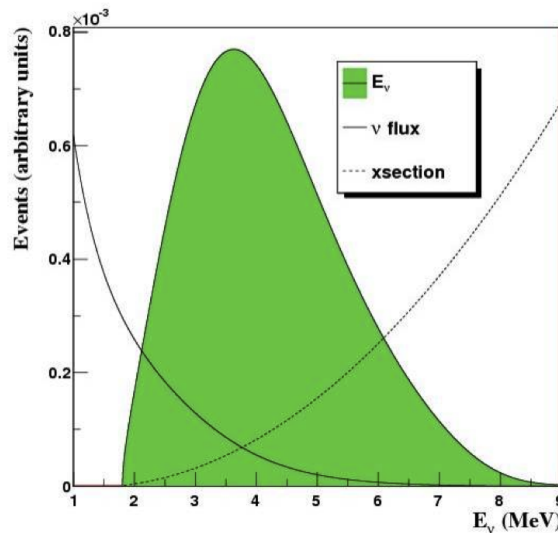


**Fig. 11:** Typical energy spectrum of antineutrinos from nuclear reactors.

of 1.8 MeV and only about  $1.5 \bar{\nu}_e$ /fission can be detected (25% of the total).

$$\bar{\nu}_e + p \rightarrow e^+ + n \quad (32)$$

Past reactor experiments were looking for the disappearance of reactor  $\bar{\nu}_e$  with the goal of solving the atmospheric problem at short baselines. All of them found negative results. The most sensitive of these experiments was the CHOOZ experiment.

CHOOZ [25] was looking for the disappearance of electron antineutrinos from the CHOOZ nuclear power plant in France in the 1990s. CHOOZ was a quite simple liquid scintillator detector doped with 0.1% Gd located 1.05 km away from the reactors. It was hosted in a cylindrical pit 7 m in diameter and height. The cylindrical steel tank was surrounded by a 75 cm thick low-radioactivity sand contained in an acrylic vessel and covered by cast iron. The target was 5 ton 0.1% Gd-loaded liquid scintillator contained in a transparent acrylic vessel. A 17 ton non-Gd-loaded liquid scintillation region contained



192 eight-inch PMTs. A muon veto region was read by two rings of 24 eight-inch PMTs.

This experiment has strongly influenced the present and upcoming reactor experiments. They had the unique opportunity to have both reactors off and periods with only one of the reactors on. This allowed a good measurement of the backgrounds.

The ratio of measured to expected events was  $1.01 \pm 2.8\%$  (stat.)  $\pm 2.7\%$  (sys.). No evidence for  $\nu_e \rightarrow \nu_\mu$  oscillations at the  $10^{-3}$  scale was found. Despite the negative result, this experiment was very sensitive to the  $\nu_e \rightarrow \nu_\tau$  oscillation. They have not observed the disappearance of electron antineutrinos but they could exclude a region in the parameter space (Fig. 12). The upper bound obtained is  $\sin^2(2\theta_{13}) < 0.12-0.2$  at 90% confidence level (CL), depending on the value of  $\Delta m_{32}^2$ .

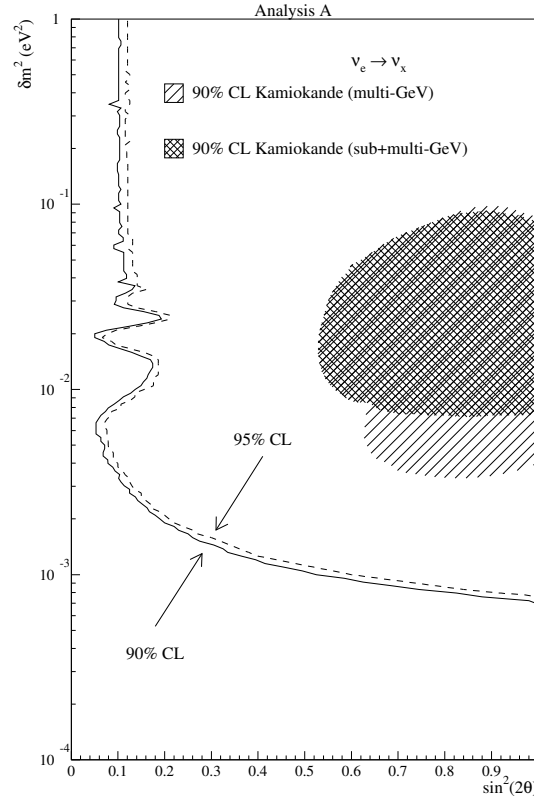


**Fig. 12:** Exclusion region in the parameter space by the CHOOZ data (from Ref. [25]).

The CHOOZ constraint is also relevant to the global interpretation of the solar and atmospheric neutrino data in the framework of three-neutrino mixing.

The neutrino oscillation in the solar range has been confirmed with reactor neutrinos by the KamLAND long-baseline reactor experiment [26]. KamLAND is a 1 kton liquid scintillator detector located at the Kamioka mine in Japan (at the old Kamiokande site) at an average distance of  $L_0 = 180$  km from 55 nuclear reactors at a depth of 2700 mwe (metres of water equivalent). They were looking for the disappearance of electron antineutrinos at  $E/L \sim 10^{-5}$  eV<sup>2</sup>, in the oscillation range indicated by the solar data. They started taking data in 2002 and finished in 2007.

The liquid scintillator is contained in a 13 m diameter spherical nylon balloon surrounded by oil in a 18 m diameter spherical stainless-steel vessel. This holds the 1879 PMTs with a photocathode coverage of 34%. A cylinder filled with water surrounds the previous volumes, being a Cerenkov veto against backgrounds (cosmic muons, gamma rays and neutrinos from the surrounding rock). This is

the largest scintillator detector ever constructed. Neutrinos are detected through the inverse beta decay reaction (Eq. (32)), the neutrons being captured in protons, giving photons of 2.22 MeV.

They reported the first evidence for the disappearance of reactor electron antineutrinos in 2002 [27]. In Fig. 13 we can see the ratio of observed over expected events (without oscillations) as a function of the distance. The deficit measured by KamLAND ( $R = 0.611 \pm 0.085$  (stat.)  $\pm 0.041$  (syst.)) for  $\bar{\nu}_e > 3.5$  MeV is compared with previous unsuccessful reactor experiments. This was consistent with the LMA region.

KamLAND presented the first evidence of spectral distortion in 2004 [28]. Figure 13 shows data compared with the non-oscillation scenario and with the best-fit oscillation spectrum as a function of the prompt event energy ( $E_{\text{prompt}} \approx E_{\bar{\nu}_e} + m_p + m_n$ ). The shaded band indicates the systematic error in the best-fit reactor spectrum above 2.6 MeV. The observed energy spectrum disagrees with the expected spectral shape in the absence of neutrino oscillation at 99.6% significance and prefers the distortion expected from the oscillation effects.

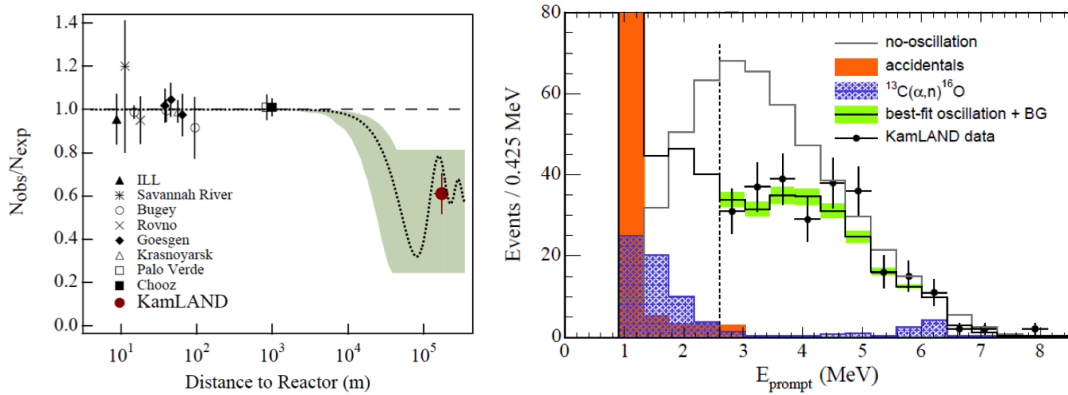


**Fig. 13:** Evidence for  $\bar{\nu}_e$  disappearance (left) and spectral distortion (right) measured by KamLAND.

KamLAND has presented new results [29] with more statistics and a lower energy threshold (0.9 MeV compared to 2.6 MeV). They have enlarged the fiducial volume and performed a campaign to purify the liquid scintillator. They have reduced the systematic uncertainty in the number of target protons and background up to 4.1–4.5%. The significance of spectral distortion is now  $> 5\sigma$ .

The KamLAND results can be interpreted in terms of  $\bar{\nu}_e$  oscillations. Figure 14 shows the allowed contours in the oscillation parameter space for solar and KamLAND data from the two-flavour oscillation analysis (assuming  $\theta_{13} = 0$ ). The solar region is in agreement with the KamLAND data. The  $\Delta m_{21}^2$  parameter is strongly determined by the KamLAND experiment.

The ratio of the background-subtracted neutrino spectrum to non-oscillation expectations as a function of  $L_0/E_\nu$  is shown in Fig. 15. We can clearly see the oscillation periods over almost two full cycles. The oscillatory signature is distorted because the reactor sources are distributed across multiple baselines.

In summary, KamLAND confirmed neutrino oscillation, providing the most precise value of  $\Delta m_{21}^2$  to date and improving the precision of  $\tan^2 \theta_{12}$  in combination with solar data. The indication of an excess of low-energy antineutrinos consistent with an interpretation as geoneutrinos persists. The scientific goals of the KamLAND experiment are now expanded towards solar neutrino detection and neutrino-less double-beta decay detection using enriched Xe.

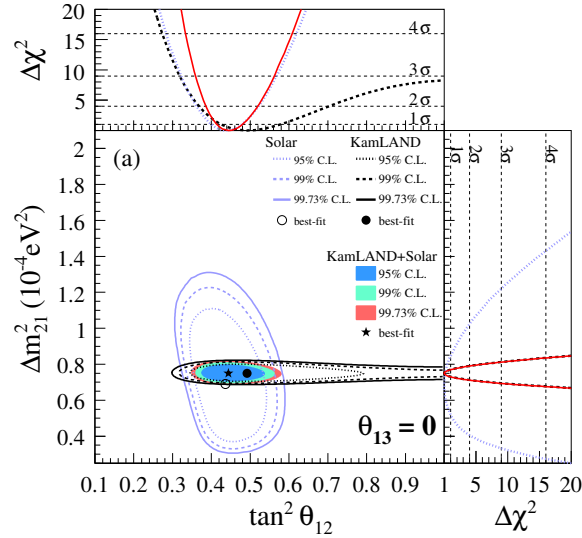


**Fig. 14:** Two-flavour neutrino oscillation analysis including solar and KamLAND data (from Ref. [29]).

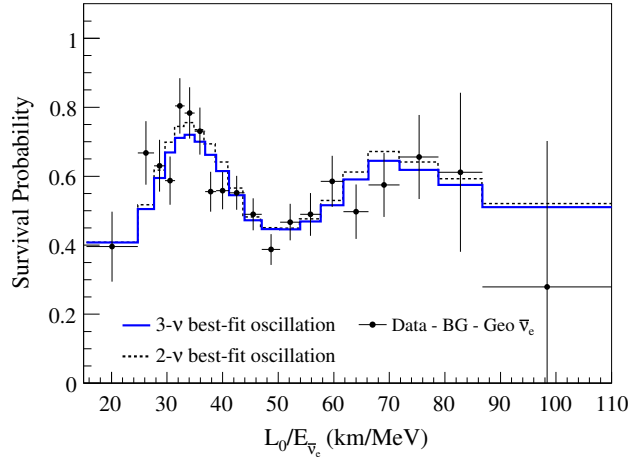


**Fig. 15:** Ratio of the observed  $\bar{\nu}_e$  spectrum to the expectation for non-oscillation versus  $L_0/E$  for the KamLAND data (from Ref. [29]).

#### 6.4 Accelerator neutrinos

Accelerator neutrinos not only have confirmed neutrino oscillations in the atmospheric region and in addition proved the appearance of flavours but also have opened new questions in neutrino physics.

Neutrinos are produced from the collision of a proton beam with a target, producing pions and kaons. Then, they are focused and decay, giving muons, electrons and neutrinos. Muons and electrons are absorbed and the surviving particles are 98% muon neutrinos and around 2% electron antineutrinos.

There are two types of searches that can be undertaken at accelerators: disappearance searches with experiments like K2K and MINOS, with not enough energy to produce the lepton in the CC reaction, and appearance searches with experiments like MiniBooNE and OPERA, with enough energy to produce the lepton. These experiments are mainly focused on the measurement of  $\Delta m_{32}^2$  and  $\theta_{23}$  and they have very limited sensitivity to  $\theta_{13}$ .

The first accelerator-based long-baseline neutrino oscillation experiment was K2K [30] starting in 1999 and running until 2004. They looked for muon neutrino disappearance using a beam provided

by KEK and detecting the oscillated neutrinos 250 km away with the SK detector. The comparison between near and far detectors allowed the measurement of 112 events, whereas 158 were expected, and a clear distortion of the energy spectrum (Fig. 16). The best-fit parameters are compatible with the SK atmospheric oscillation results.

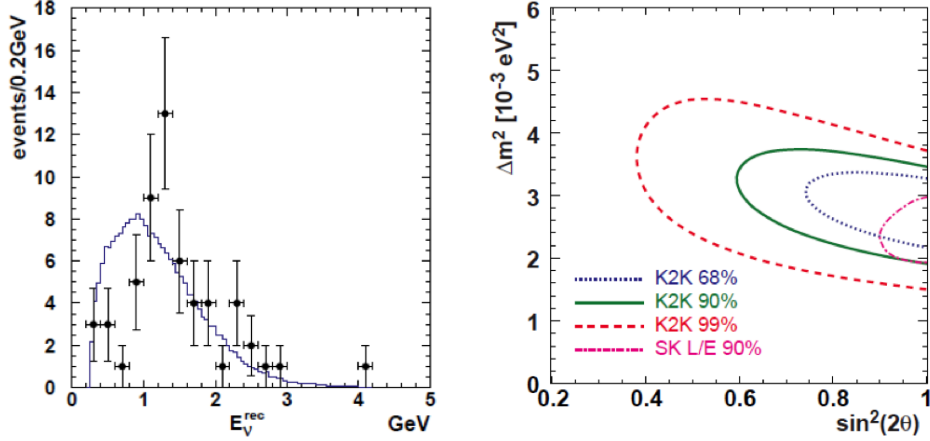


**Fig. 16:** (left) Distribution of  $\nu_\mu$  events in K2K as a function of the reconstructed neutrino energy and (right) allowed regions from the analysis of K2K data compared to the  $L/E$  SK analysis.

More recently, the MINOS long-baseline experiment [31] has presented a positive result on neutrino oscillations. MINOS is composed of two similar magnetized steel/scintillator calorimeters to look for the disappearance of muon neutrinos from the NUMI beam at Fermilab. The 1.5 kton near detector is located near the source at Fermilab and the 5 kton far detector is placed 735 km away in the Soudan mine.

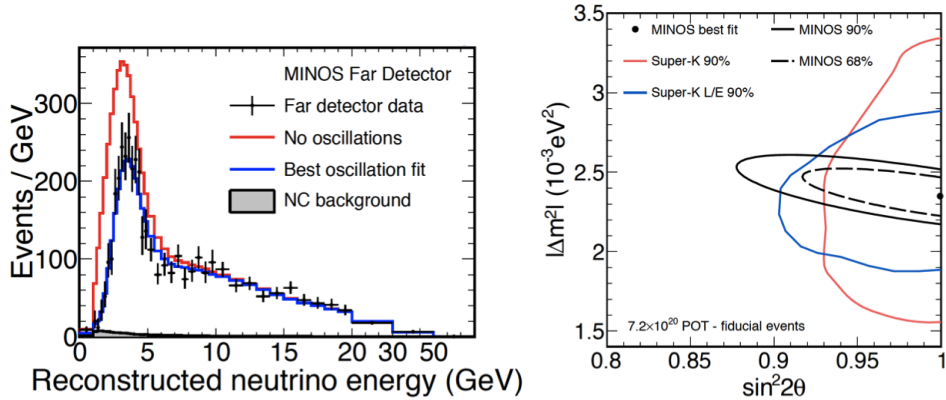


**Fig. 17:** (left) Distribution of the neutrino energy at the far MINOS detector compared to the non-oscillation case and (right) the corresponding allowed regions in the oscillation parameter space (from Ref. [32]).

Figure 17 shows the MINOS far detector data with a significant deficit compared to the non-oscillation case and very good agreement with the  $\nu_\mu$ - $\nu_\tau$  oscillation scenario. The allowed region in the parameter space is shown in this plot together with the results from SK  $L/E$  analysis and K2K. The measurement of  $\Delta m_{32}^2$  is dominated by MINOS, while the angle  $\theta_{23}$  is essentially determined by SK.

A similar study to that discussed previously has been performed on the antineutrino dataset [33]. MINOS is also able to distinguish between muon neutrinos and antineutrinos. A total of  $1.7 \times 10^{20}$

protons on target (POT) were accumulated between September 2009 and March 2010. The reconstructed energy spectrum of  $\bar{\nu}_\mu$  CC events at the far detector shows a deficit in the low-energy region. The best-fit oscillation parameters to  $\bar{\nu}$  data are shown in Fig. 18. We see the corresponding contours for neutrino and antineutrino oscillations. Antineutrinos favour a slightly higher  $\Delta m^2$  than neutrino data, which could violate CPT. Anyway, the results are compatible at  $2\sigma$  and more data are being taken to understand if this is a statistical fluctuation or not. Matter effects cannot explain this discrepancy (too small effect).

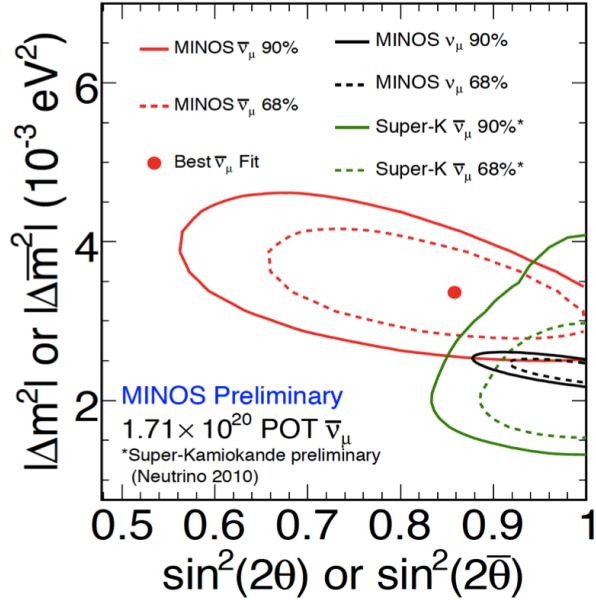


**Fig. 18:** Allowed regions in the oscillation parameter space for neutrino and antineutrino data (from Ref. [33]).

A subdominant transition  $\nu_\mu \rightarrow \nu_e$  would be expected if  $\theta_{13} \neq 0$ . MINOS was optimized for muon identification, and thus the reconstruction of electromagnetic showers is difficult. They use an artificial neural network technique for this analysis. Recent results looking for  $\nu_e$  appearance have shown a very small excess of data ( $0.7\sigma$  over the expected background) [34]. This measurement is also consistent with no  $\nu_e$  appearance. A limit has been set around the CHOOZ value. Since MINOS is sensitive to matter effects, they have different limits depending on the sign of  $\Delta m^2$  (Fig. 19).

Among the short-baseline accelerator neutrino experiments, LSND is the first experiment that claimed the observation of neutrino oscillation appearance [35]. They were taken data from 1993 to 1998 looking for the appearance of electron antineutrinos in a muon antineutrino beam produced at Los Alamos National Laboratory. The detector was a tank filled with 167 ton of dilute liquid scintillator, located about 30 m from the neutrino source. The experiment observed an excess of events above the MC predictions (at  $3.8\sigma$ ) that could be interpreted in terms of  $\bar{\nu}_\mu \rightarrow \bar{\nu}_e$  oscillations. The corresponding  $\Delta m^2$  is in the range shown in Fig. 20. These results created a huge controversy because they are not compatible with atmospheric and solar oscillations since they cannot be explained assuming three-flavour oscillations.

The region of parameter space that is favoured by the LSND observations has been partly tested by other experiments like KARMEN [36] with negative results on neutrino oscillations. KARMEN excluded part of the LSND region. Another experiment is needed to definitively confirm this excess or not.

This is the case of the MiniBooNE experiment, designed to test the neutrino oscillation interpretation of the LSND signal. This experiment was proposed in 1997 and started running in 2002. MiniBooNE [37] is an 800 ton mineral oil Cerenkov detector placed at 540 m from the neutrino source and

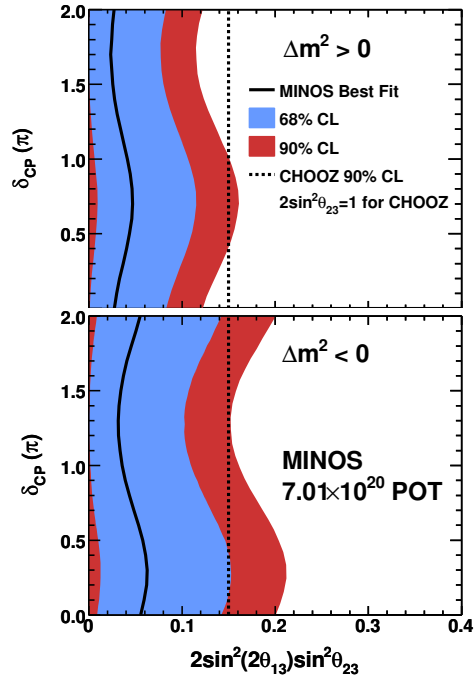


**Fig. 19:** Values of  $2 \sin^2(2\theta_{13}) \sin^2 \theta_{23}$  and  $\delta_{CP}$  that produce a number of candidate events in the far MINOS detector consistent with the observation for (top) the normal hierarchy and (bottom) the inverted hierarchy. Black lines are the best fit and red (blue) regions show the 90% (68%) CL intervals (from Ref. [34]).

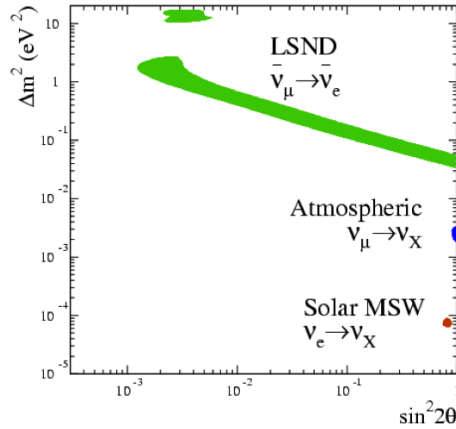


**Fig. 20:** Allowed regions in the parameter space including atmospheric, solar and LSND data.

uses the  $\nu_\mu$  beam produced by the Booster Neutrino Beamline at Fermilab. The  $L/E$  baseline is similar to the LSND, but the baseline and neutrino energies are one order of magnitude higher. Therefore, MiniBooNE systematic errors are completely different. They also have higher statistics and they are taking data in both neutrino and antineutrino modes.

Figure 21 shows the MiniBooNE results for  $\nu_\mu - \nu_e$  oscillations in terms of the reconstructed energy distribution of  $\nu_e$  candidates [38]. Points are data with the statistical error and the histogram is the background prediction with systematic errors. For the analysis region between 475 MeV and 1.25 GeV,

there is no evidence of oscillations. Data are consistent with background. MiniBooNE has excluded two neutrino oscillations in the LSND region at 98% CL. However, in the low-energy part of the spectrum (between 200 and 475 MeV) they have found a sizeable excess of data. The excess at low energy has a significance of  $1.7\sigma$  or  $3.4\sigma$  and is incompatible with LSND-type oscillations. The source of this excess remains unknown.

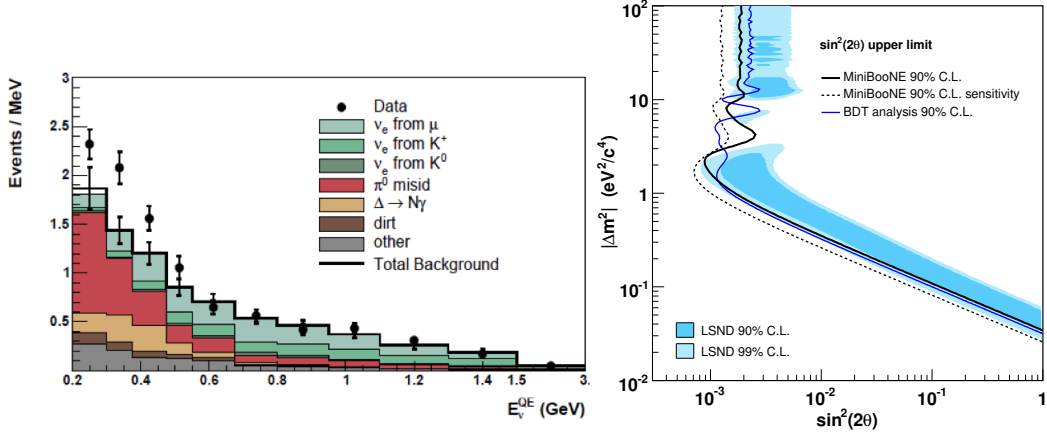


**Fig. 21:** (left) Neutrino energy distribution for  $\nu_e$  CCQE data and background and (right) 90% CL limit (thick curve) and sensitivity (dashed curve) for events with energy  $> 475$  MeV within a two-neutrino  $\nu_\mu \rightarrow \nu_e$  oscillation model (from Ref. [38]).

MiniBooNE has also reported results from the search for  $\bar{\nu}_\mu - \bar{\nu}_e$  oscillations [39]. For the oscillation study, no contribution from the low-energy neutrino mode excess has been accounted for in the  $\bar{\nu}$  prediction. In Fig. 22 the  $\bar{\nu}_e$  charged-current quasi-elastic (CCQE) energy for data and background events is shown. From 200 to 3000 MeV there is a total excess of  $43.2 \pm 22.5$  events. The excess is present in the low ( $< 475$  MeV) and high ( $> 475$  MeV) energy regions.

Many checks have been performed on the data to ensure that backgrounds are correctly estimated. Any single background would have to be increased by more than  $3\sigma$  to explain the observed excess of events. On the right-hand plot of Fig. 22 the 90, 95 and 99% CL contours for  $\bar{\nu}_\mu \rightarrow \bar{\nu}_e$  oscillations in the energy range  $> 475$  MeV are shown. The allowed regions are in agreement with LSND allowed regions. The probability of background-only fit relative to the best oscillation fit is 0.5%. Comparison between MiniBooNE and LSND as a function of  $L/E$  also shows consistency between both results.

The source of the excess observed by MiniBooNE at low energy and the difference found between neutrino and antineutrino results are still under study.

CNGS [40] is the neutrino beam facility in Europe. It is mainly a  $\nu_\mu$  beam from the CERN SPS with a mean energy of  $\sim 17$  GeV, a 4%  $\bar{\nu}_\mu$  contamination and a 0.9% ( $\nu_e + \bar{\nu}_e$ ) contamination. Two experiments, OPERA and ICARUS, are located in the LNGS laboratory in Italy, 730 km away from the neutrino source. Their main goal is to detect  $\nu_\mu \rightarrow \nu_\tau$  transitions in appearance mode. Physics operations started in 2007 and they have provided neutrino beams in 2008, 2009 and 2010.

OPERA looks for  $\nu_\tau$  CC interactions through the measurement of  $\tau$  decay kinks in different channels. The detector consists of a large set of emulsion-lead targets combined with electronic detectors and a magnetic spectrometer. This technique provides a very good spatial resolution of the order of the micrometres.

In August 2009 the OPERA collaboration presented the first  $\nu_\tau$  neutrino candidate [41]. With their statistics, they expected 0.5  $\nu_\tau$  candidates. The statistical significance of the measurement of a first  $\nu_\tau$  candidate is  $2.36\sigma$ . For five years of data taking at the nominal CERN performance of  $4.5 \times 10^{19}$  POT, they expect to detect 10  $\tau$  events.

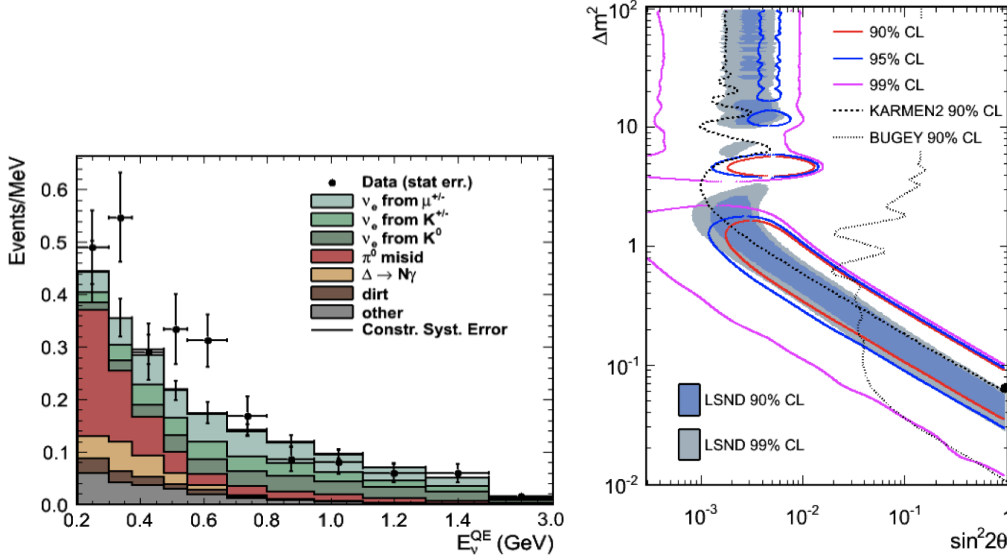


**Fig. 22:** (left) Neutrino energy distribution for  $\bar{\nu}_e$  CCQE data and background and (right) the 90, 95 and 99% CL allowed regions for events with energy  $> 475$  MeV within a two-neutrino  $\bar{\nu}_\mu \rightarrow \bar{\nu}_e$  oscillation model (from Ref. [39]).

The ICARUS T600 detector at LNGS [42] is a 600 ton LAr TPC providing 3D imaging of any ionizing event. T600 is presently taking data and has smoothly reached the optimal working conditions. They have already observed neutrino interactions. The first data analysis is ongoing, together with the development of fully automated reconstruction software. They expect to measure one or two  $\tau$  events in the next two years.

## 6.5 Global analysis of oscillation data

In previous sections, all the current neutrino oscillation results have been summarized. The three pieces of neutrino oscillation evidence have been explained corresponding to three different values of mass-squared differences. The mixing of three standard neutrinos can only explain two of the anomalies. The explanation of the three sets of data would require the existence of sterile  $\nu$  species, since only three light neutrinos can couple to the  $Z^0$  boson.

In the case of the solar and atmospheric neutrino indications, several experiments agree on the existence of the effect and they have been confirmed by terrestrial reactor and accelerator experiments. Therefore, the standard scenario is to consider three-neutrino mixing without the LSND result. Several attempts have been made in the literature to accommodate also LSND data (include a fourth sterile neutrino, break CPT symmetry, make neutrinos and antineutrinos have different masses). However, the present phenomenological situation is that none of these explanations can successfully describe all the neutrino data.

Table 2 summarizes the present values of the oscillation parameters from a recent global three-flavour neutrino oscillation analysis of the experimental data [43]. The upper (lower) row corresponds to normal (inverted) mass hierarchy.

There are two possible mass orderings, which we denote as normal ( $\Delta m_{32}^2 > 0$ ) and inverted ( $\Delta m_{32}^2 < 0$ ). The two orderings are often referred to in terms of  $\text{sgn}(\Delta m_{32}^2)$ .

As you may see, not all of the neutrino oscillation parameters have been measured: the value of the  $\theta_{13}$  angle, the sign of the  $\Delta m_{32}^2$  (mass hierarchy) and the CP violation phase are still unknown.



**Table 2:** Neutrino oscillation parameter summary (from Ref. [43]).

Parameter	Best fit $\pm 1\sigma$	$2\sigma$	$3\sigma$
$\Delta m_{21}^2$ ( $10^{-5}$ eV $^2$ )	$7.59_{-0.18}^{+0.20}$	7.24–7.99	7.09–8.19
$\Delta m_{32}^2$ ( $10^{-3}$ eV $^2$ )	$2.45 \pm 0.09$ $-(2.34_{-0.09}^{+0.10})$	2.28–2.64 $-(2.17-2.54)$	2.18–2.73 $-(2.08-2.64)$
$\sin^2 \theta_{12}$	$0.312_{-0.015}^{+0.017}$	0.28–0.35	0.27–0.36
$\sin^2 \theta_{23}$	$0.51 \pm 0.06$ $0.52 \pm 0.06$	0.41–0.61 0.42–0.61	0.39–0.64
$\sin^2 \theta_{13}$	$0.010_{-0.006}^{+0.009}$ $0.013_{-0.007}^{+0.009}$	$\leq 0.027$ $\leq 0.031$	$\leq 0.035$ $\leq 0.039$

Past and present experiments tried to measure the  $\theta_{13}$  mixing angle without success. We only have an upper limit on its value, indicating that this angle must be very small. However, the best-fit point of this parameter is not zero. There are independent hints for  $\theta_{13} > 0$  computed using different data ranging between  $1.4\sigma$  and  $2.8\sigma$ .

Figure 23 illustrates the interplay of the various datasets in the plane of  $\sin^2 \theta_{13}$  and  $\Delta m_{31}^2$ . The latest T2K results have not been considered in this analysis.

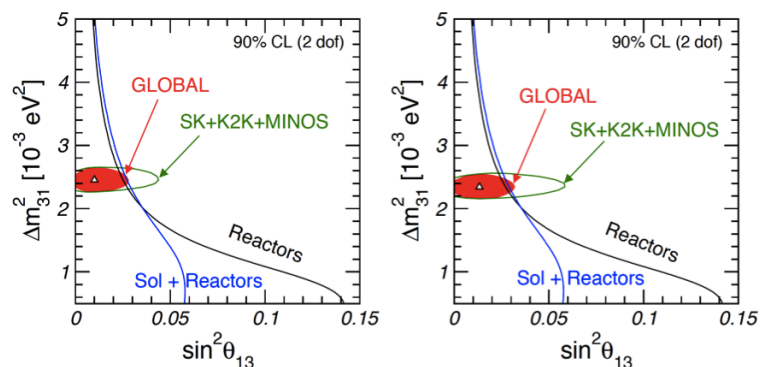


**Fig. 23:** Bound on  $\sin^2 \theta_{13}$  using global data, corresponding to (left) normal hierarchy and (right) inverted hierarchy (from Ref. [43]).

## 7 Current and future neutrino oscillation experiments

In the previous section I provided a summary of the present situation in terms of experimental neutrino oscillation results and data analysis. As pointed out, there are still many questions to be answered by forthcoming neutrino oscillation experiments in the next few years and further in the future.

The main topics that will be addressed by the current and near-future experiments are:

- measurement of  $\theta_{13}$  mixing angle;
- accurate measurements of other oscillation parameters ( $\Delta m_{32}^2$ ,  $\theta_{23}$ , is  $\theta_{23}$  maximal?);
- understanding of LSND/MiniBooNE anomalies;

- understanding of differences observed between neutrinos and antineutrinos in accelerator experiments;
- searching for CP violation in the leptonic sector; and
- searching for the sign of  $\Delta m_{32}^2$ .

Current experiments that will try to study these questions are the accelerator experiments MINOS, OPERA, ICARUS and MiniBOONE, which will continue their operation to accumulate more statistics, and the new ones T2K in Japan and NO $\nu$ A in the USA. Concerning reactor neutrinos, there are essentially three new reactor experiments that would like to measure  $\theta_{13}$ : Double Chooz in France is already taking data, RENO in Korea is coming soon, and Daya Bay in China a bit later. In addition, more news on SK and Borexino concerning natural sources will be reported.

The first goal of the near-future experiments is to measure the  $\theta_{13}$  mixing angle. There are essentially two ways of studying this parameter: with neutrino accelerator long-baseline experiments or reactor experiments.

The long-baseline accelerator experiments will try to measure the  $\theta_{13}$  mixing angle by looking for the appearance of electron neutrinos in a muon neutrino beam generated at great distance from the detector. The main problem to measure  $\theta_{13}$  with accelerator experiments is that the oscillation probability depends on several parameters in such a way that the measurement of  $\theta_{13}$  will be affected by correlations and degeneracies between parameters (their sensitivity will be reduced). Owing to the long baseline, they can also be sensitive to matter effects.

However, reactor neutrino experiments are unique for providing an unambiguous determination of  $\theta_{13}$ . The electron antineutrino disappearance probability does not depend on the CP phase nor on the sign of  $\Delta m_{32}^2$ . It depends essentially on  $\theta_{13}$  (only has a weak dependence on  $\Delta m_{21}^2$ ). Therefore, unlike appearance experiments, they do not suffer from parameter degeneracies. Moreover, the matter effects are negligible due to the small distances. So, they will provide a clean measurement of the mixing angle. In addition to this, they can help to solve the  $\theta_{23}$  degeneracy (the octant of  $\theta_{23}$  if not maximal,  $\theta_{23} > \pi/4$  or  $< \pi/4$ ) combined with accelerator experiments.

The experimental challenges of neutrino accelerator experiments are related to the neutrino beam intensity, the contamination of other flavours in the neutrino beam, the uncertainties on the neutrino flux properties and the neutrino–nucleus interactions. On the other hand, reactor neutrino experiments have a pure antineutrino flux without flavour contamination, the flux is known at few per cent level, and the cross-section is high, so the needed detectors are smaller (and cheaper compared to accelerator experiments). However, they need to deal with backgrounds and reduce the systematic uncertainties to provide a precise measurement. On the other hand, accelerator experiments are able to provide other measurements like CP-violation. Anyway, both kinds of experiments are necessary. They provide independent and complementary information.

## 7.1 New reactor experiments

The main goal of the new reactor experiments is to measure the  $\theta_{13}$  mixing angle. In order to achieve this, several improvements with respect to previous reactor measurements are needed. It will be necessary to increase the statistics. More powerful reactors are desired, longer exposure and larger detector mass. On the other hand, backgrounds should be further reduced with a better detector design: using veto detectors and external shields against muons and external radioactivity. Finally, an important reduction of the systematic uncertainties is fundamental to reach the high precision needed. It could be achieved by performing relative measurements using two identical detectors and comparing them to minimize the reactor errors. A detailed calibration programme will be needed.

Reactor experiments will look for the disappearance of electron antineutrinos coming from nuclear reactors. The corresponding oscillation probability (Eq. (33)) essentially depends on  $\Delta m_{32}^2$  and  $\sin^2 2\theta_{13}$ . The second term corresponds to a second oscillation amplitude dominated by solar parameters

and has been measured with the KamLAND experiment:

$$P(\nu_e \rightarrow \nu_e) = 1 - \sin^2 2\theta_{13} \sin^2 \left( \frac{\Delta m_{32}^2 L}{4E_\nu} \right) - \cos^4 \theta_{13} \sin^2 2\theta_{12} \sin^2 \left( \frac{\Delta m_{21}^2 L}{4E_\nu} \right). \quad (33)$$

Figure 24 shows the survival probability as a function of the distance of detection for a typical reactor neutrino energy of 4 MeV. Owing to the low neutrino energies, reactor neutrino experiments are disappearance experiments located at short distances in order to maximize the disappearance probability. At  $\sim 1$ – $2$  km from the neutrino source, a small antineutrino deficit is expected over a large neutrino flux. High precision will be necessary to measure the mixing angle.

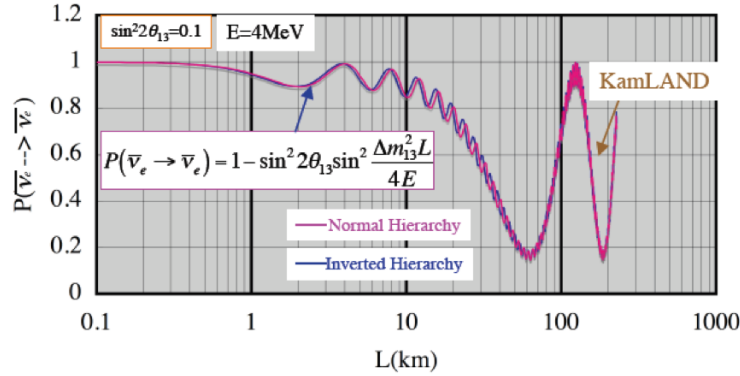


**Fig. 24:** Survival oscillation probability for a typical reactor neutrino experiment.

The reactor antineutrinos are detected through the inverse beta decay reaction (Eq. (32)) giving a prompt signal due to the  $e^+$  annihilation and a delayed signal from the neutron capture ( $\sim 30 \mu s$  later) giving photons of  $\sim 8$  MeV in the case of capture in Gd. In the case of H, the delayed signal happens  $200 \mu s$  later and the photons are of 2 MeV. The spectrum peaks around 3.6 MeV and neutrino energy threshold is 1.8 MeV.

The signature of a neutrino interaction can be mimicked by two types of background events: accidental or correlated. All backgrounds are linked to the cosmic muon rate and detector radiopurity. Compared to CHOOZ, backgrounds can be reduced with a better detector design and *in situ* measurements.

The accidental events occur when a neutron-like event by chance falls in the time window of  $\sim 100 \mu s$  after an event in the scintillator with an energy above 0.5–0.7 MeV. The positron-like signal comes from natural radioactivity of the rock or of the detector materials, in general, dominated by the PMT radioactivity. The delayed background (neutron-like signal) comes from neutron captures on Gd. They are energy deposits over 6 MeV isolated in time from other deposits.

The correlated background are events that mimic both parts of the coincidence signal: one single process induces both a fake positron and a neutron signal. They come from fast neutrons induced by cosmic muons, which slow down by scattering in the scintillator, deposit more than 0.5 MeV visible energy and are captured on Gd. Correlated background can also be produced by long-lived isotopes like  $^8\text{He}$ ,  $^9\text{Li}$  or  $^{11}\text{Li}$ , which undergo beta decay with neutron emission.

There are several reactor neutrino experiments that are looking to measure the  $\theta_{13}$  angle with sensitivities on  $\sin^2 2\theta_{13}$  up to 0.01: Double Chooz in France, RENO in Korea and Daya Bay in China. Table 3 summarizes the three reactor neutrino experiments in progress. Double Chooz [44] is the most advanced of the three reactor experiments, since it is already taking data. The three detectors are quite similar with slight variations between them.

**Table 3:** Comparison between reactor neutrino experiments.

Experiment	Location	Th. power (GW)	Distances near/far (m)	Depth near /far (mwe)	Target mass (ton)	Expect. sensit. (3 yr)
Double Chooz	France	8.5	400/1050	115/300	10/10	0.03
RENO	Korea	16.4	290/1380	120/450	15/15	0.02
Daya Bay	China	11.6 (17.4)	360(500)/ 1985(1613)	260/910	40×2/80	0.01

The antineutrinos used in Double Chooz are produced by the pair of reactors (type N4) located at the Chooz-B nuclear power station in France. The maximum operating thermal power of each core amounts to 4.27 GW. The idea of Double Chooz is to use two almost identical neutrino detectors of medium size, containing 10.3 m<sup>3</sup> of liquid scintillator target doped with 0.1% of gadolinium. The neutrino laboratory of the first CHOOZ experiment is located 1.050 km from the two cores. The far detector is already installed at this site. The far site is shielded by about 300 mwe of rocks. In order to cancel the systematic errors originating from the lack of knowledge of the  $\bar{\nu}_e$  flux and spectrum, as well as to reduce the set of systematic errors related to the detector and event selection procedure, a second detector will be installed close to the nuclear cores, at  $\sim 400$  m.

The Double Chooz detector consists of concentric cylinders (Fig. 25). A target cylinder of 1.2 m radius and 2.5 m height, providing a volume of 10.3 m<sup>3</sup>, is filled with a liquid scintillator doped with gadolinium (1 g/l). This is the volume for neutrino interactions. Surrounding the target we have the gamma-catcher region of 22.6 m<sup>3</sup> containing non-loaded liquid scintillator with the same optical properties as the  $\bar{\nu}_e$  target (light yield, attenuation length). This is an extra volume for gamma interaction. This region is needed to measure the gammas from the neutron capture on Gd, to measure the positron annihilation and to reject the background from fast neutrons. Surrounding the gamma-catcher acrylic tank there is a 1 m thick non-scintillating (oil) buffer contained in a stainless-steel tank. The goal of this region is to decrease the level of accidental background mainly from the contribution from PMT radioactivity. The photomultiplier tubes are mounted from the interior surface of the buffer vessel and they collect the light from the target volume and the gamma-catcher. They are 390 10-inch PMTs per detector to cover  $\sim 13\%$ . Then a 50 cm thick inner veto region is filled with liquid scintillator to tag the muon-related background events. Finally, a 15 cm thick steel shielding will protect the detector from natural radioactivity of the rocks around the pit with a significant gamma reduction. An additional muon outer veto (plastic scintillator planes) will be required to help identify muons, which could cause neutrons or other cosmogenic backgrounds.

The statistical error in CHOOZ was 2.8% while in Double Chooz in three years it is expected to be  $\sim 0.5\%$ . The fiducial volume has been increased with respect to CHOOZ and longer data taking is expected. Concerning the systematic errors, in CHOOZ the total systematic error was 2.7%, dominated by the reactor antineutrino flux and spectrum uncertainties (1.9%). In Double Chooz the uncertainty related to the reactor is cancelled by using two identical detectors. The relative normalization between the two detectors is the most important source of error. The goal of Double Chooz is to reduce the overall systematic uncertainty to 0.6%. Table 4 summarizes the expected systematic errors in Double Chooz.

The Double Chooz far detector started to take data at the end of 2010. Figure 26 shows an internal view of the detector with all PMTs installed inside the buffer volume and, on the right, the first signals of a few photoelectrons contained in the inner detector.

The expected Double Chooz  $\sin^2 2\theta_{13}$  sensitivity as a function of time is shown in Fig. 27 in the case when no signal is observed. Double Chooz will operate in two phases. In the first one, after 1.5 years of data taking with the far detector, a limit of  $\sin^2 2\theta_{13} < 0.06$  at 90% CL can be reached. Using both detectors, it is possible to measure  $\sin^2 2\theta_{13}$  up to 0.05 at  $3\sigma$  or to obtain a limit down to 0.03 at

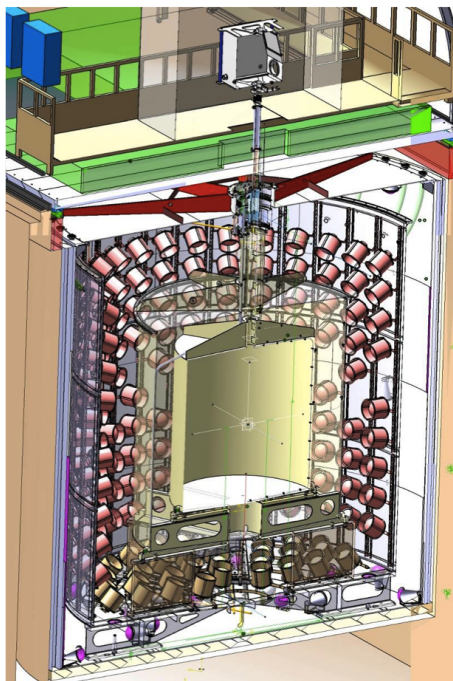


**Fig. 25:** Sketch of the Double Chooz detector.

**Table 4:** Summary of Double Chooz systematic errors.

	<b>CHOOZ</b>	<b>Double Chooz</b>
Reactor uncertainties ( $\nu$ flux and reactor power)	2.1%	< 0.1%
Number of protons	0.8%	< 0.2%
Detector efficiency	1.5%	< 0.5%
<b>Systematic error</b>	<b>2.7%</b>	<b>&lt; 0.5%</b>

90% CL after three years of data taking.

The RENO [45] reactor neutrino experiment is under construction at YongGwang in South Korea. The plant consists of six equally spaced reactors in line spanning  $\sim 1.3$  km. The total average thermal power is  $\sim 16.4$  GWth. One near detector and one far detector are placed in the iso-flux line from the reactors. The near detector is located  $\sim 290$  m from the cores' barycentre with an overburden  $\sim 120$  mwe. The far detector is at 1380 m surrounded by 450 mwe. The design of the RENO detectors is quite similar to the Double Chooz one. The inner detector is bigger (16 ton) and the main difference is the muon veto system, which is a 30 cm concrete vessel filled with water observed by 60 PMTs.

The goal of the experiment is to have a systematic error of the order of 0.5% and a statistical error  $\sim 0.3\%$ . The expected limit is  $< 0.02$  and the discovery reach at  $3\sigma$  up to 0.04 after three years of data taking. Both detectors are being commissioned. They expect to start data taking with the two detectors at the end of 2011.

A third reactor neutrino experiment, Daya Bay [46], is under construction in China, at the Ling Ao and Daya Bay nuclear power plants. The power plant complex is now composed of two pairs of reactors, Daya Bay and Ling Ao-I. Other two reactors named Ling Ao-II are under construction and should be operational in 2011. Each core yields 2.9 GW, thus the site is 11.6 GW and will be 17.4 GW.

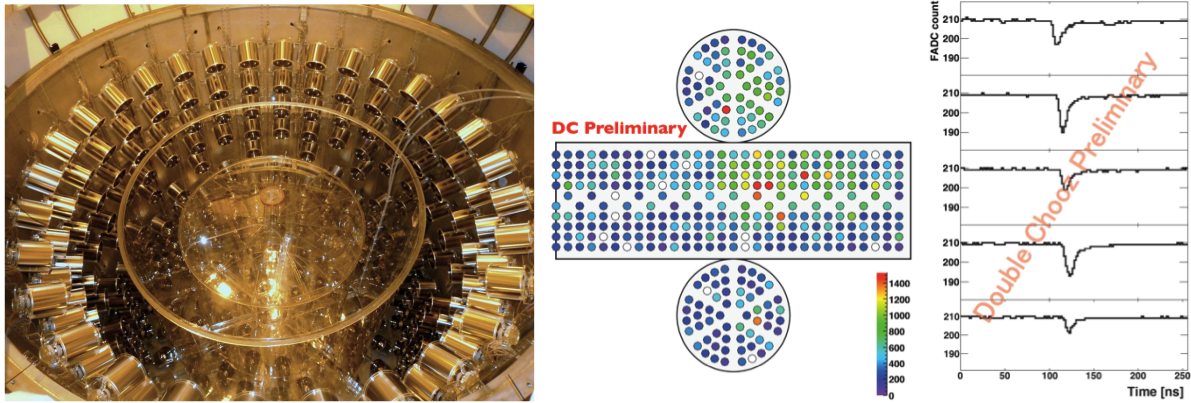


**Fig. 26:** (left) Internal view of the Double Chooz detector with the PMTs installed and (right) one event of a few photoelectrons contained in the inner detector.

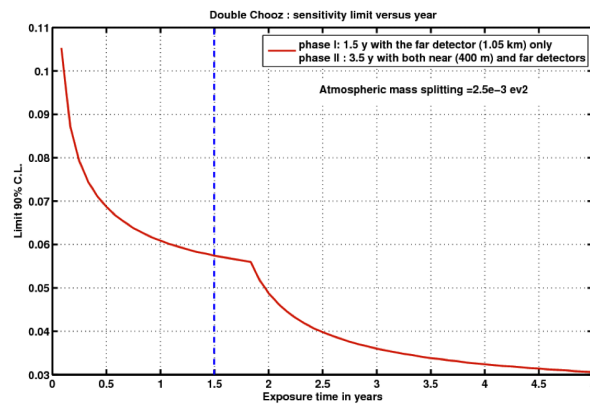


**Fig. 27:** Expected Double Chooz sensitivity on  $\sin^2 2\theta_{13}$ .

Near detectors are needed in near sites to monitor the different reactors. Two detectors will be installed at  $\sim 360$  m from Daya Bay, two detectors at  $\sim 500$  m from Ling Ao, and four far detectors at 1.6 km from the barycentre of Ling Ao sites and  $\sim 2$  km from Daya Bay. Each detector contains 20 ton of liquid scintillator doped with Gd. Horizontal tunnels connect the detector halls for cross-calibration. The design of the detector is very similar to the Double Chooz one except for the shielding. The detectors of each site are submerged into a swimming pool filled with purified water giving protection against radiation and fast neutrons. The water pool is instrumented with PMTs to read the Cerenkov light to tag muons together with resistive plate chambers (RPCs) placed on top of the water pool. This system is under production. The excavation of access tunnels and experimental halls is nearing completion. Two near detectors are completed. The expected systematic error is 0.38%. They have the ambitious idea of swapping the detectors of different sites, moving them through the tunnels to reduce the systematic errors from relative detector normalization to 0.12%. The expected sensitivity at 90% CL with three years of data taking (assuming a systematic error of 0.4%) is 0.01. Daya Bay plans to start taking data with the first near site in summer 2011 and with the three sites operational at the end of 2012.

## 7.2 New accelerator experiments

Complementary to reactors, new accelerator experiments will measure neutrino oscillations in the next few years. Their main goal is to look for  $\nu_e$  appearance in a muon neutrino beam. The approximate

formula for the oscillation probability can be written as

$$P(\nu_e \rightarrow \nu_\mu) \approx s_{23}^2 \sin^2 2\theta_{13} \sin^2 \left( \frac{\Delta m_{32}^2 L}{4E_\nu} \right) + P_{\text{sol}}(\theta_{12}, \Delta m_{21}^2) \pm \sin 2\theta_{13} F_{\text{solar}} F(\sin 2\theta_{23}, |\Delta m_{32}^2|) F(\delta_{\text{CP}}, \Delta m_{32}^2). \quad (34)$$

The first term corresponds to atmospheric oscillations, the second one is the solar one and there is an interference term, which has the information on the  $\delta_{\text{CP}}$  phase and also dependence on the sign of  $\Delta m_{32}^2$ . The + (−) sign applies to neutrinos (antineutrinos), respectively.

Accelerator experiments will try to measure the  $\theta_{13}$  mixing angle, provide more precise measurements of the atmospheric parameters and in principle look for CP-violation,

$$P(\nu_\alpha \rightarrow \nu_\beta) - P(\bar{\nu}_\alpha \rightarrow \bar{\nu}_\beta) \neq 0 \quad (\alpha \neq \beta), \quad (35)$$

and matter effects.

There are two effects, one from the CP phase and another from matter effects, that produce differences between neutrinos and antineutrinos. We need to disentangle these two effects using different experimental set-ups. At short distances, CP-violating effects dominate, while at long distances, matter effects completely hide CP-violating effects. They can be distinguished by the different neutrino energy dependence. In order to achieve this, an improvement of the present beams is needed: with much higher intensities and almost monochromatic beams.

New detectors at accelerators are located off-axis in order to reduce the beam energy and have a more monochromatic beam. This technique allows experiments to pick the energy corresponding to the maximum oscillation signal and, at the same time, to get rid of the high-energy part contributing most of the background. The  $\nu_e$  contamination from the beam could be reduced below the 1% level.

In Fig. 28 the neutrino energy spectrum is shown for different off-axis degrees. The energy peak is reduced and becomes narrower by increasing the off-axis angle. In addition, the contamination of  $\nu_e$  from the beam is greatly reduced. The problem with this technique is the reduced rate. Thus, large detectors and intense proton sources are needed.

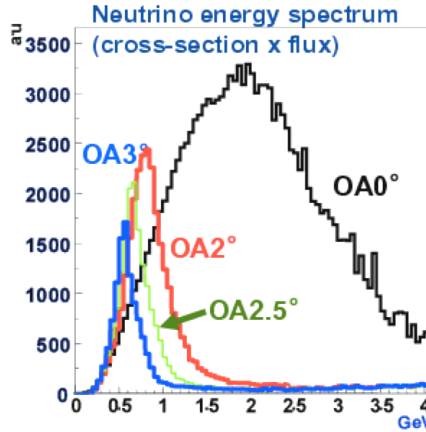


**Fig. 28:** Neutrino energy spectrum variation as a function of the off-axis angle.

In accelerator experiments, the main neutrino signal will be CCQE interactions. They will look for the muon or electrons coming from these reactions. They have to deal with backgrounds coming essentially from the  $\nu_e$  contamination of the beam and from  $\pi^0$  production in neutral currents.

The main long-baseline project that has begun operation this year is T2K [47]. The neutrino beam is produced in the accelerator complex of J-PARC in Japan and it will travel 295 km to Kamioka,

where the SK detector is located. They will use near and far detectors to control the beam and measure the oscillations. Both detectors are  $2.5^\circ$  off neutrino beam axis. This gives a neutrino beam energy of  $\sim 600$  MeV. Owing to the short distance, this experiment is not sensitive to matter effects but can provide information on CP if  $\theta_{13}$  is not too small.

T2K will have different detectors along the beam line. A muon monitor is located after the beam dump and measures the direction and intensity of the beam. It is used as a proton beam detector, target monitor and horn monitor. The INGRID on-axis detector, at 280 m from the target, is made of steel and scintillator layers and measures the intensity and direction of the neutrino beam. It monitors the beam using muons from CC neutrino interactions. The ND280 off-axis near detector is a magnetized detector inside the former UA1 magnet donated by CERN to this experiment (0.2 T). It is composed of several subdetectors: a  $\pi^0$  detector, a tracker made of fine-grain detectors and TPCs to detect charged particles and measure their momentum, and an electromagnetic calorimeter. The Side Muon Range Detector will detect muons and measure their momenta. This detector measures the neutrino flux and spectrum before oscillations, different interaction cross-sections and also the backgrounds for  $\nu_e$  appearance. Finally, the SK detector expects 10  $\nu_\mu$  events per day at full beam power.

T2K completed its first run in the first half of 2010. A total of  $3.23 \times 10^{19}$  protons were delivered at 30 GeV. The beam was working at 50 kW of power. T2K has analysed both  $\nu_\mu$  and  $\nu_e$  samples. For the  $\nu_\mu$  disappearance analysis,  $\nu_\mu$  is consistent with previous disappearance experiments. In the appearance  $\nu_e$  channel, they have observed six  $\nu_e$  candidates, and the expected number of events in a three-flavour neutrino oscillation scenario with  $|\Delta m_{32}^2| = 2.4 \times 10^{-3} \text{ eV}^2$ ,  $\sin^2 2\theta_{23} = 1$  and  $\sin^2 2\theta_{13} = 0$  was  $1.5 \pm 0.3$  (syst.) [48]. At 90% CL, the data are consistent with  $0.03$  ( $0.04$ )  $< \sin^2 2\theta_{13} < 0.28$  ( $0.34$ ) for  $\delta_{\text{CP}} = 0$  and normal (inverted) hierarchy.

Their goal for 2011 was to accumulate  $150 \text{ kW} \times 10^7 \text{ s}$  by July and increase the beam power. However, due to the March 2011 earthquake, the experiment has been somewhat delayed. More data are required to firmly establish  $\nu_e$  appearance and to determine the  $\theta_{13}$  angle.

Assuming the beam running at 750 kW for five years, Fig. 29 shows the expected sensitivity that T2K plans to reach for  $\sin^2 2\theta_{13}$  as a function of  $\Delta m_{32}^2$  at 90% CL and for different systematic errors, assuming  $\delta_{\text{CP}} = 0$ . They could be sensitive down to 0.01 at 90% CL. The final sensitivity will depend on the value of  $\delta_{\text{CP}}$ .

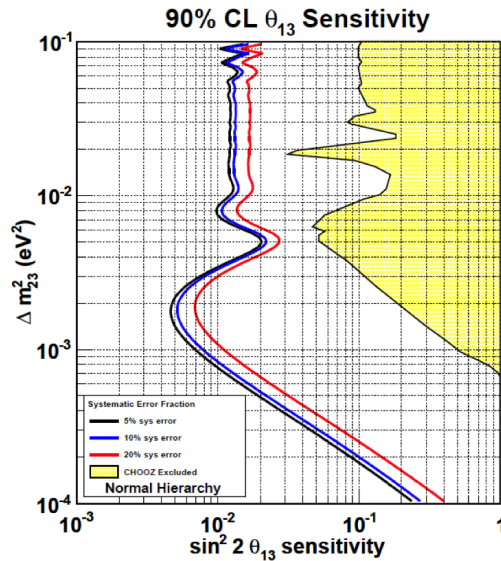


**Fig. 29:** Expected sensitivity of the T2K experiment to  $\sin^2 2\theta_{13}$  for five years of data taking with a 750 kW beam assuming  $\delta_{\text{CP}} = 0$  and normal mass hierarchy (from Ref. [49]).



There is another approved experiment that will start its operation in 2013: the NO $\nu$ A experiment (NUMI Off-axis Neutrino Appearance) [50]. They will search for  $\nu_e$  appearance using an upgraded version of the NUMI beam at 700 kW with two identical detectors: a 220 ton near detector located close to the source at 1 km and a 15 ton far detector at 810 km away at Ash River, Minnesota, USA. They will use active tracking liquid scintillator calorimeters with very good electron identification capability.

The unique feature of this experiment is that, depending on the value of  $\theta_{13}$ , NO $\nu$ A could be the only approved experiment with sensitivity to determine the neutrino mass hierarchy. The detectors will be placed off-axis at  $0.8^\circ$  to tune the neutrino energy to 2 GeV and maximize the  $\nu_e$  appearance. They can run in the neutrino and antineutrino modes. The NuMI beam will be upgraded from 320 kW to 700 kW during the shutdown of 2012.

NO $\nu$ A plans to run for three years in neutrino mode and three years in antineutrino mode. They plan to take advantage of the large matter effects. Figure 30 shows the NO $\nu$ A sensitivity to matter effects depending on the  $\delta_{CP}$  value. The mass ordering can only be solved by NO $\nu$ A alone in this region of the parameter space, if the hierarchy is normal. For the rest of the parameter space, we need to combine these measurements with other experiments, like T2K, which will improve the sensitivity a bit. NO $\nu$ A plans to have the far detector completed in October 2013.

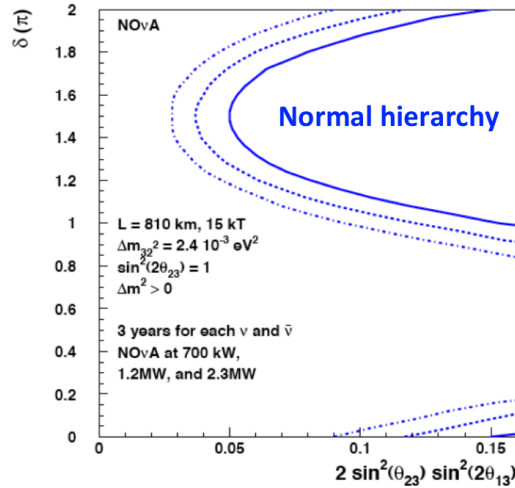


**Fig. 30:** The 95% resolution of the mass ordering as a function of  $\delta_{CP}$  for six years of NO $\nu$ A running split evenly between neutrinos and antineutrinos for different beam powers in the case of normal mass ordering (from Ref. [50]).

In the next few years, it is possible that these experiments will provide a measurement of  $\theta_{13}$  mixing angle, if  $\sin^2 2\theta_{13} > 0.01$  and solve the  $\theta_{23}$  degeneracy. However, they will have limited sensitivity to CP-violation and matter effects. More than 70% of the parameter space will not be accessible.

The ultimate goals of the future generation will depend on these measurements, but in principle they will focus on CP-violation (new measurements are needed to solve degeneracies) and on the mass hierarchy. To achieve these measurements, many improvements are needed from the experimental point of view: We will need upgraded beams that are more energetic, more powerful and more pure. We will need huge detectors (one order of magnitude bigger), with more granularity and energy resolution. And, to solve the degeneracies, we will need different energies, baselines (longer baselines to enhance matter effects) and detection channels.

New facilities and experiments are being proposed that can realize some (or all) of the pending issues:

- (a) *Superbeams* are more powerful versions of conventional pion decay-based beams. They could be obtained with new megawatt proton sources. They will need to be coupled with huge detectors at longer distances to explore matter effects. In these facilities, the main beam consists of  $\nu_\mu$  and the experiments will search for both  $\nu_\mu$  disappearance and  $\nu_e$  appearance. Several possibilities are under study: a CERN upgraded beam to large detectors located in European underground laboratories (LAGUNA), a new beamline from an upgraded accelerator complex (2.3 MW beam power) to be sent to a large detector located in the DUSEL underground laboratory (1300 km), and an upgraded version of the J-PARC beam (1.66 MW) to T2HK in Japan or another detector in Korea.
- (b) *Beta-beams* are very pure  $\nu_e$  or  $\bar{\nu}_e$  beams made by allowing accelerated radioactive ions to decay in a storage ring. Both  $\nu_e$  disappearance and  $\nu_\mu$  appearance are sought. However,  $\nu_\mu$  disappearance cannot be studied.
- (c) *Neutrino factories* are facilities where muons are produced by pion decay, cooled, injected into a storage ring and allowed to decay in straight sections. This provides a very clean  $\nu_\mu$  and  $\bar{\nu}_e$  beams (or vice versa) with well-known energy spectrum. The dominant search is the appearance of “wrong-sign” muons from the oscillation of  $\bar{\nu}_e$ . Other oscillation channels can also be observed. They will need detectors with capability to distinguish between  $\mu^+$  and  $\mu^-$ .

Figure 31 (from Ref. [51]) compares the  $\sin^2 2\theta_{13}$  discovery reach at  $3\sigma$  for different future facilities.

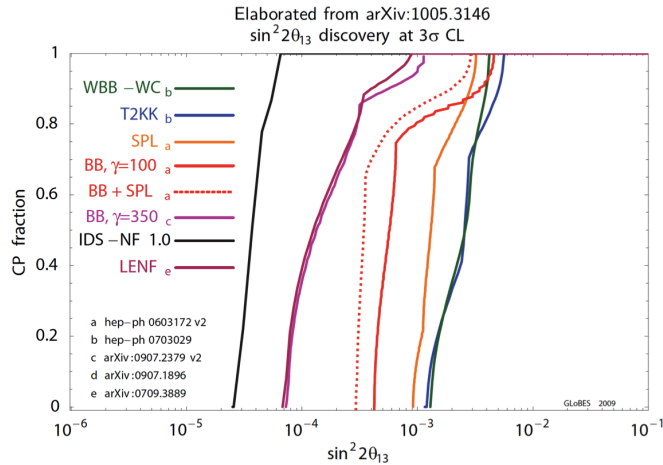


**Fig. 31:** Physics reach of different future facilities in  $\sin^2 2\theta_{13}$  (from Ref. [51]).

## 8 Direct measurements of neutrino mass

The properties of neutrinos and especially their rest mass play an important role in cosmology, particle physics and astroparticle physics. Neutrino oscillation experiments provide compelling evidence that neutrinos are massive but they cannot provide the absolute mass value.

There are two complementary approaches for measuring the neutrino mass in laboratory experiments: one is the precise spectroscopy of beta decay at its kinematic endpoint, and the other is the search for neutrinoless double-beta decay ( $0\nu\beta\beta$ ).

The  $0\nu\beta\beta$  process requires the neutrino to be a Majorana particle and the effective Majorana mass  $m_{\beta\beta}$  can be determined as

$$m_{\beta\beta} = \left| \sum_i U_{ei}^2 m_i \right|. \quad (36)$$

This is the coherent sum of all mass eigenstates  $m_i$  with respect to the PMNS mixing matrix  $U_{ei}$ ;  $m_{\beta\beta}$  depends on complex CP phases with the possibility of cancellations. Therefore, this implies a model-dependent determination of the Majorana mass.

Experiments investigating single-beta decay offer a direct and model-independent method to determine the absolute neutrino mass;  $m_{\nu_e}$  is determined as an incoherent sum of all mass eigenstates according to the PMNS matrix:

$$m_{\nu_e}^2 = \sum_i |U_{ei}|^2 m_i^2. \quad (37)$$

The experiments looking for  $0\nu\beta\beta$  decay have the potential to probe  $m_{\beta\beta}$  in the 20–50 meV region. New single- $\beta$  experiments will increase the sensitivity on  $m_{\nu_e}$  by one order of magnitude to 200 meV.

The basic principle applied in the single-beta decay model-independent method is based on kinematics and energy conservation. The idea is to measure the spectral shape of beta decay electrons close to their kinematic endpoint (Eq. (38)), where  $E_0 - E$  is small and the mass term  $m_i$  becomes significant. A non-zero neutrino mass will not only shift the endpoint but also change the spectral shape:

$$\frac{d\Lambda_i}{dE} = Cp(E + m_e)(E_0 - E)\sqrt{(E_0 - E)^2 - m_i^2} F(E, Z)\Theta(E_0 - E - m_i^2). \quad (38)$$

Here  $E_0$  is the maximum energy,  $F(E, Z)$  is the Fermi function and  $m_i$  is the neutrino mass.

The experimental requirements for doing this measurement are having a low-endpoint  $\beta$  source for a large fraction of electrons in the endpoint region, high energy resolution and very low background. Figure 32 shows the evolution of the experimental bounds on neutrino masses with time.

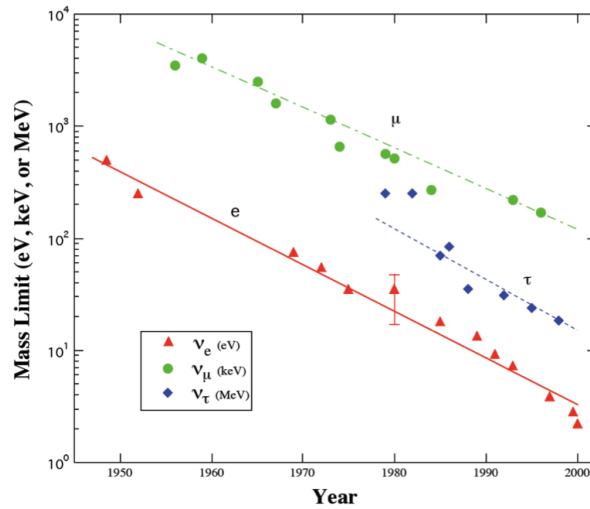
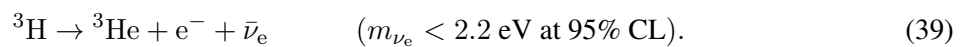


**Fig. 32:** Limits on neutrino masses versus year (from Ref. [2]).

At present the best experimental limits from single-beta decay have been determined by the Mainz and Troitsk experiments [52] through the tritium beta decay:



The direct limits on the other two neutrino masses are much weaker. The muon neutrino mass limit ( $m_{\nu_\mu} < 170 \text{ keV}$ ) has been determined from the endpoint spectrum of the pion decay  $\pi^+ \rightarrow \mu^+ \nu_\mu$ . The tau neutrino mass ( $m_{\nu_\tau} < 18.2 \text{ MeV}$ ) has been measured using the tau hadron decay  $\tau \rightarrow 5\pi \nu_\tau$ .

There are two complementary experimental approaches (calorimetry and spectroscopy) for measuring the neutrino mass from single- $\beta$  decays with different systematics. In the calorimeter approach, the source is identical to the detector. The best choice for the source is  $^{187}\text{Re}$  crystal bolometers and the entire beta decay energy is measured as a differential energy spectrum.  $^{187}\text{Re}$  has the lowest endpoint (2.47 keV) but, due to its rather long half-life ( $4.3 \times 10^{10}$  yr), the activity is rather low. Since bolometers are modular, their number can be scaled in order to increase the sensitivity. This approach is being followed in the MARE experiment [53]. In the spectrometer approach, an external tritium source is used. Electrons are magnetically or electrostatically selected and transported to the counter. The kinetic energy of the beta electrons is analysed as an integral spectrum by an electrostatic spectrometer. The material is a high-purity molecular tritium source with a low endpoint at 18.6 keV and a short half-life providing high activity. This approach has reached its ultimate size and precision in the KATRIN experiment [54].

The KATRIN set-up (Fig. 33) extends over 70 m. KATRIN uses a molecular gaseous tritium source. Electrons emitted by the  $\text{T}_2$  decay are guided by strong magnetic fields (3.6 T in the source and 5.6 T in the transport section) to the transport section and finally to the spectrometer section. The gas flow is retained by 14 orders of magnitude by active and cryogenic pumping. The pre-spectrometer can be used to transmit only electrons with energies close to the  $\text{T}_2$  endpoint. Only electrons of the endpoint region would enter the main spectrometer for precise energy analysis. The low-energy part of the spectrum is filtered. Then, when electrons enter the spectrometer, the magnetic field drops by several orders of magnitude. Only electrons able to cross the potential in the spectrometer are counted. The main spectrometer offers a resolution of 0.93 eV for 18.6 keV electrons by applying a magnetic field ratio of 1/20 000. The selected electrons are counted in a final detector (Si PIN diodes with energy resolution of 1 keV). The main inconvenience here is that the source is external and results suffer from many systematic uncertainties, since the final energy of the electrons needs to be corrected for the energy lost in the different steps.

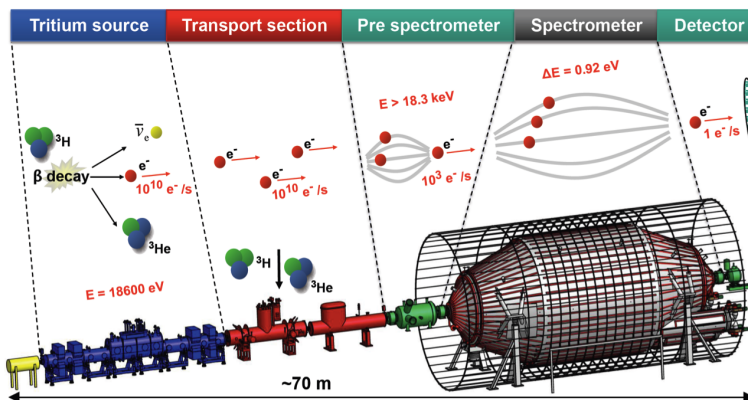


Fig. 33: Set-up of the KATRIN experiment.

The main spectrometer is going to follow a test programme in 2011 and they plan to have the system integrated for late 2012. After three years of data taking, they plan to arrive at a sensitivity for the neutrino mass  $< 0.2$  eV at 90% CL or they could be able to detect a neutrino mass up to 0.35 eV at  $5\sigma$  significance.

The MARE experiment wants to make a direct and calorimetric measurement of the  $\nu_e$  mass with sub-eV sensitivity. They plan to use  $^{187}\text{Re}$  (or  $^{163}\text{Ho}$ ) as beta emitter and they will measure all the energy released in the decay except the  $\nu_e$  energy. The systematic uncertainties from the external electron source are eliminated. On the other hand, because they detect all the decays occurring over the entire beta decay spectrum, the source activity must be limited to avoid pulse pile-up at the endpoint. Thus, the statistics at the endpoint will be limited. They use thermal microcalorimeters whose absorbers contain the beta

decay isotope with a low  $Q$ -value ( $\sim 2.5$  keV). They plan to improve the energy resolution to 1–2 eV. The MARE project is subdivided into two phases: MARE I is an R&D phase focused on the choice of the best isotope and the best detector technology for the final experiment. They will use 300 bolometers and plan to take data for three years to investigate masses between 2 and 4 eV. MARE II will be the final large scale of the detector with sub-eV sensitivity (improving the mass sensitivity by one order of magnitude) and investigate the KATRIN region. They plan to use 50 000 bolometers and five years of data taking.

New ideas have recently come up to measure the neutrino mass. Project 8 [55] aims to make use of radio-frequency techniques to measure the kinetic energy of electrons from a gaseous tritium source. When a relativistic electron moves in a uniform magnetic field, cyclotron radiation is emitted. The characteristic frequency is inversely proportional to the energy of the electron. An array of antennas would capture the cyclotron radiation emitted by the electrons when moving and, by measuring the frequency, the energy of the electron could be obtained. The authors claim that they can obtain sensitivities of 0.1 eV. They are now preparing a proof-of-principle experiment to show the feasibility of detecting electrons and determining their kinetic energy.

## 9 Neutrinoless double-beta decay

Direct information on neutrino masses can also be obtained from neutrinoless double-beta decay ( $0\nu\beta\beta$ ) searches. This process violates the total lepton number and requires Majorana neutrinos. Therefore, the detection of such a process would prove that neutrinos are their own antiparticles.

The double-beta ( $\beta\beta$ ) decay process is allowed when single-beta decay is energetically forbidden or strongly suppressed. The double-beta decay is characterized by a nuclear process that changes the charge  $Z$  in two units while leaving the total mass  $A$  unchanged:

$$(A, Z) \rightarrow (A, Z + 2) + 2e^- + 2\bar{\nu}_e. \quad (40)$$

For this, it is necessary that the mass  $m(A, Z) > m(A, Z + 2)$ . This condition is fulfilled in several nuclei, with lifetimes between  $10^{18}$  and  $10^{21}$  years.

In the  $0\nu\beta\beta$  decay process, only two electrons are emitted:

$$(A, Z) \rightarrow (A, Z + 2) + 2e^-. \quad (41)$$

The process can be mediated by the exchange of a light Majorana neutrino or other particles. The existence of  $0\nu\beta\beta$  decay requires Majorana neutrino mass, no matter what the actual mechanism is and a violation of the total lepton number conservation. A limit on the half-life of this process implies a limit on the effective Majorana neutrino mass.

In the case of  $\beta\beta$  decay, we should observe a continuous energy spectrum corresponding to the two electrons up to the endpoint of the decay (Fig. 34). In the case of  $0\nu\beta\beta$  decay, we should only see a line coming from the two electron energies since no neutrinos are carrying away part of the energy of the process. In that sense, to observe and be sensitive to  $0\nu\beta\beta$ , we need good energy resolution to separate this line from the possible background (including the possible  $\beta\beta$  decay up to the  $Q$ -value).

The inverse half-life ( $T_{1/2}^{-1}$ ) of the neutrinoless double-beta decay rate is proportional to the square of the effective Majorana mass and also depends on the phase space factor ( $G^{0\nu}$ ) and the nuclear matrix elements ( $M^{0\nu}$ ), which are difficult to evaluate. While the phase space can be calculated reliably, the computation of the nuclear matrix is subject to uncertainty. This would give a factor  $\sim 3$  uncertainty in the derived  $m_{\beta\beta}$  values:

$$T_{1/2}^{-1} \simeq G^{0\nu} |M^{0\nu}|^2 \langle m_{\beta\beta} \rangle^2. \quad (42)$$

The effective neutrino mass  $m_{\beta\beta}$  depends directly on the assumed form of lepton number-violating interactions. The simplest one is a light Majorana neutrino exchange. Assuming this, the effective

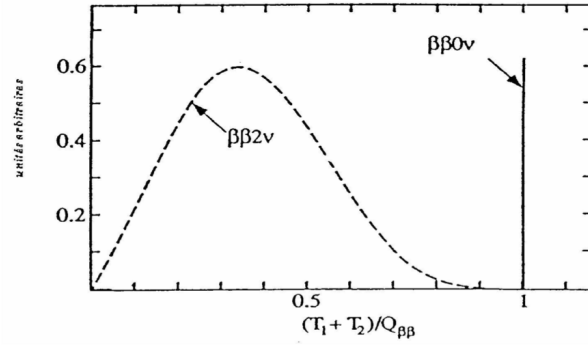


**Fig. 34:** Energy spectrum of  $\beta\beta$  and  $0\nu\beta\beta$  processes.

Majorana neutrino mass can be written as the sum of the mass eigenvalues multiplied by the mixing matrix elements and the CP phases:

$$m_{\beta\beta} = |m_1 c_{12}^2 c_{13}^2 + m_2 s_{12}^2 c_{13}^2 e^{i\alpha_1} + m_3 s_{13}^2 e^{i\alpha_2}|. \quad (43)$$

The individual neutrino masses can be expressed in terms of the smallest neutrino mass and the mass-squared differences. For the normal mass hierarchy (NH),

$$m_3 \simeq \sqrt{\Delta m_{\text{atm}}^2} \gg m_2 \simeq \sqrt{\Delta m_{\text{sun}}^2} \gg m_1, \quad (44)$$

the effective mass is

$$\langle m_{\beta\beta} \rangle^{\text{NH}} \simeq |(m_1 c_{12}^2 + \sqrt{\Delta m_{\text{sun}}^2} s_{12}^2 e^{i\alpha_1}) c_{13}^2 + \sqrt{\Delta m_{\text{atm}}^2} s_{13}^2 e^{i\alpha_2}| \quad (45)$$

For the inverted mass hierarchy (IH), the smallest neutrino mass is  $m_3$ ,

$$m_2 \simeq m_1 \simeq \sqrt{\Delta m_{\text{atm}}^2} \gg m_3, \quad (46)$$

and the effective mass can be written as

$$\langle m_{\beta\beta} \rangle^{\text{IH}} \approx \sqrt{\Delta m_{\text{atm}}^2} c_{13}^2 |c_{12}^2 + s_{12}^2 e^{i\alpha_1}|. \quad (47)$$

In the quasi-degenerate case (QD),

$$m_0^2 \equiv m_1^2 \simeq m_2^2 \simeq m_3^2 \gg \Delta m_{\text{atm}}^2, \quad (48)$$

the effective mass is

$$\langle m_{\beta\beta} \rangle^{\text{QD}} \approx m_0 |(c_{12}^2 + s_{12}^2 e^{i\alpha_1}) c_{13}^2 + s_{13}^2 e^{i\alpha_2}|. \quad (49)$$

Given our present knowledge of the neutrino oscillation parameters, one can derive the relation between the effective Majorana mass and the mass of the lightest neutrino, as shown in Fig. 35.

In principle, a determination of the Majorana mass would allow us to distinguish between these regions. The three different mass hierarchies allowed by the oscillation data result in different projections. The width of the innermost dark bands reflects the uncertainty introduced by the unknown Majorana phases. Because of the overlap of the different mass scenarios, a measurement of  $m_{\beta\beta}$  in the degenerate or hierarchical ranges would not determine the hierarchy. Naturally, if  $m_{\beta\beta} < 0.01$  eV, normal hierarchy becomes the only possible scenario.

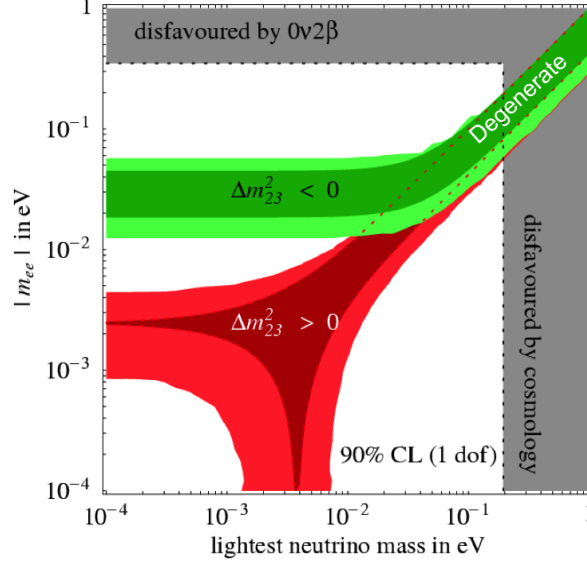


**Fig. 35:** Effective Majorana neutrino mass as a function of the smallest neutrino mass.

The most sensitive double-beta experiments, Heidelberg–Moscow HM-1 and IGEX, have used  $^{76}\text{Ge}$  as source and detector, and reach sensitivities around 0.3 eV in the effective neutrino mass. Both collaborations have reported almost the same upper limit on the half-life of  $1.6 \times 10^{25}$  yr, corresponding to a mass range of 0.33 to 1.3 eV [56].

However, part of the Heidelberg–Moscow collaboration claimed in 2001 the observation of the  $0\nu\beta\beta$  process [57] with five enriched high-purity  $^{76}\text{Ge}$  detectors (10.96 kg of active volume). New results were presented in 2004 with collected statistics of 71.7 kg yr [58]. The background achieved in the energy region of  $0\nu\beta\beta$  decay is very low (0.11 events/kg yr keV). The confidence level for the neutrinoless signal was improved to  $4.2\sigma$  with a  $T_{1/2} = 0.69\text{--}4.18 \times 10^{25}$  yr corresponding to  $\langle m_{\beta\beta} \rangle = 0.24\text{--}0.58$  eV. This would imply a degenerate neutrino mass hierarchy.

This result has been much criticized and remains controversial (in contradiction with HM-1 and IGEX experiments, only part of the collaboration agrees with the result, not all the background peaks are explained) and needs to be confirmed or refuted by other experiments.

The latest reanalysis of data from 1990 to 2003 shows a  $6\sigma$  excess of counts at the decay energy, which corresponds to a Majorana neutrino mass of  $0.32 \pm 0.03$  eV at 68% CL (Fig. 36).

## 9.1 Experimental detection

Neutrinoless double-beta decay is a very rare process. The half-life sensitivity of this process depends on whether there is background or not. The sensitivity (without background) is proportional to the exposure (mass  $M \times$  time of measurement  $t$ ) and the isotopic abundance  $a$ ; with background, it is inversely proportional to the background rate  $B$  and the energy resolution  $\Delta E$ :

$$\begin{aligned} T_{1/2} &\propto aM\epsilon t && \text{(background free),} \\ T_{1/2} &\propto a\epsilon\sqrt{\frac{Mt}{\Delta E B}} && \text{(background limited).} \end{aligned} \quad (50)$$

Therefore, the basic experimental requirements for detecting this process are a large and highly efficient source mass, excellent energy resolution and an extremely low background in the  $0\nu\beta\beta$  peak region.

The neutrinoless double-beta decay experiments can be classified into two types, depending on whether or not the source is the same as the detector. The first experimental approach is calorimetric

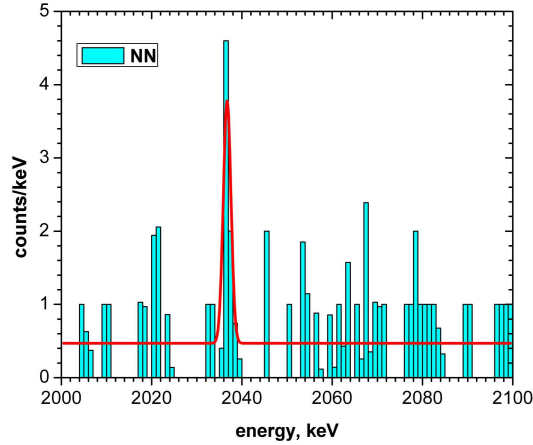


**Fig. 36:** The claim by the Heidelberg–Moscow experiment to have observed the  $0\nu\beta\beta$  process at  $> 6\sigma$  (from Ref. [59]).

detectors, where the source is the detector. They have good energy resolution and good scaling-up, but modest background discrimination. Thus, strong requirements on radiopurity and shielding are needed. The semiconductors, cryogenic bolometers, scintillators and liquid and gaseous Xe TPCs are in this category. The second approach involves detectors where the source is different from the detector. This is the case for the combined tracking and calorimetry (tracko-cal) experiments, where foils of  $\beta\beta$  source are surrounded by a tracking detector that provides direct detection of the two electron tracks emitted in the decay. They have a moderate energy resolution and are difficult to scale-up. However, they can provide information on the event topology.

The main goals of the future  $0\nu\beta\beta$  experiments will be to reach sensitivities of the order of  $\langle m_{\beta\beta} \rangle \sim 0.01\text{--}0.1$  eV (IH mass region) using different isotopes and different experimental techniques. Table 5 shows a summary of the forthcoming  $0\nu\beta\beta$  experiments.

**Table 5:** Overview of upcoming  $0\nu\beta\beta$  experiments.

Experiment	Isotope	Mass (kg)	Technique	Sensit. $T_{1/2}^{0\nu}$ (yr)	Status
GERDA	$^{76}\text{Ge}$	40	ionization	$2 \times 10^{26}$	in progress
Majorana	$^{76}\text{Ge}$	30	ionization	$1 \times 10^{26}$	in progress
COBRA	$^{116}\text{Cd}, ^{130}\text{Te}$	t.b.d.	ionization	t.b.d.	R&D
CUORE	$^{130}\text{Te}$	200	bolometers	$6.5 \times 10^{26}$	in progress
EXO	$^{136}\text{Xe}$	200	liquid TPC	$6.4 \times 10^{25}$	in progress
NEXT	$^{136}\text{Xe}$	100	gas TPC	$1.8 \times 10^{26}$	in progress
SNO+	$^{150}\text{Nd}$	liquid scintillator	56	$4.5 \times 10^{24}$	in progress
KamLAND-Zen	$^{136}\text{Xe}$	liquid scintillator	400	$4 \times 10^{26}$	in progress
SuperNEMO	$^{82}\text{Se}, ^{150}\text{Nd}$	100	tracko-cal	$1\text{--}2 \times 10^{26}$	in progress

The GERDA and Majorana experiments will search for  $0\nu\beta\beta$  in  $^{76}\text{Ge}$  using arrays of high-purity germanium detectors. This is a well-established technique offering outstanding energy resolution (better than 0.2% full width at half-maximum (FWHM) at the  $Q_{\beta\beta}$  value) and high efficiency ( $\sim 80\%$ ) but limited methods to reject backgrounds.



The GERDA detector [60] is made of an 86% enriched pure naked  $^{76}\text{Ge}$  crystal array immersed in LAr and surrounded by 10 cm of lead and 2 m of water. In phase I, they will operate the refurbished HM and IGEX enriched detectors ( $\sim 18$  kg). They will verify or reject the Heidelberg–Moscow claim with the same detectors. They expect a background rate of the order of 0.01 counts/keV kg yr. In phase II, they will add 20 kg of segmented detectors to arrive at a background level of  $\sim 0.001$  counts/keV kg yr. Depending on the outcome, there could be a phase III, merging GERDA and Majorana detectors, to reach a mass of the order of 1 ton and test the IH mass region.

The Majorana experiment [61] is located in Sanford Laboratory and will be composed of 30 kg of enriched  $^{76}\text{Ge}$  crystals with a passive Cu and Pb shielding providing a low background. They anticipate a background rate of 0.001 counts/keV kg yr.

The COBRA experiment [62] aims to search for the  $0\nu\beta\beta$  decay of  $^{116}\text{Cd}$  and  $^{130}\text{Te}$  with CdZnTe semiconductors. It is currently in the R&D phase and they have a test set-up working at the Gran Sasso laboratory. The idea is to use an array of CdZnTe room-temperature semiconductors. The exploration of pixellated detectors will add tracking capabilities to the pure energy measurements and even further background reduction by particle identification. A scientific proposal is foreseen by the end of 2012.

CUORICINO was an experiment at the Gran Sasso laboratory working from 2003 to 2008. It was composed by cryogenic bolometers of  $\text{TeO}_2$  crystals. The  $0\nu\beta\beta$  decay was not observed and the experiment has been able to set the world's most stringent lower limit for the half-life for  $0\nu\beta\beta$  in  $^{130}\text{Te}$ , namely,  $T_{1/2} \geq 2.8 \times 10^{24}$  yr at 90% CL [63].

The CUORE detector [64] will consist of an array of 988  $\text{TeO}_2$  crystals that contain 27%  $^{130}\text{Te}$  as the source of  $0\nu\beta\beta$  with  $\sim 200$  kg of  $^{130}\text{Te}$  for a total detector mass of about 740 kg. The crystals will be cooled inside a specially built dilution refrigerator – one of the world's largest – to a temperature of  $\sim 10$  mK, at which point they have such a small heat capacity that the energy deposited by individual particles or gamma rays in a crystal produces a temporary, measurable rise of its temperature. The measured temperature pulses will be used to construct an energy spectrum of the interactions occurring inside the crystals, and the spectrum is then inspected for a small peak at 2527 keV. The next project goal for CUORE will be the construction and operation of CUORE-0, the first 52-crystal tower produced by the CUORE detector assembly line. The CUORE-0 tower will be installed in the existing CUORICINO cryostat, and it will take data for the next two years while the 19 CUORE towers are assembled. CUORE-0 is primarily intended to serve as a test of the CUORE detector assembly protocols and to verify the functionality of the experimental components, but it will nevertheless represent a significant measurement: it will be comparable in size to CUORICINO, yet its energy spectrum will have a lower background due to improvements in materials and assembly procedures. The advantages and disadvantages of the technique are similar to those of germanium experiments, with about the same energy resolution and efficiency for the signal. The expected sensitivity for a background of 0.001 counts/keV kg yr and  $\Delta E = 5$  keV is  $\sim 6.5 \times 10^{26}$  yr.

SNO+ [65] proposes to fill the Sudbury Neutrino Observatory (SNO) with liquid scintillator. A mass of several tens of kilograms of  $\beta\beta$  decaying material can be added to the experiment by dissolving a neodymium salt in the scintillator. The natural abundance in the  $^{150}\text{Nd}$  isotope is 5.6%. Given the liquid scintillator light yield and photocathode coverage of the experiment, a modest energy resolution performance (about 6% FWHM at  $Q_{\beta\beta}$ ) is expected. This could be compensated by large quantities of isotope and low backgrounds. They plan to use enriched Nd to increase the mass.

KamLAND-Zen [66] plans to dissolve 400 kg of  $^{136}\text{Xe}$  in the liquid scintillator of KamLAND in the first phase of the experiment, and up to 1 ton in a projected second phase. Xenon is relatively easy to dissolve (with a mass fraction of more than 3% being possible) and also easy to extract. The major modification to the existing KamLAND experiment is the construction of an inner, very radiopure and very transparent balloon to hold the dissolved xenon. The balloon, 1.7 m in radius, would be shielded from external backgrounds by a large, very radiopure liquid scintillator volume. While the energy resolution at  $Q_{\beta\beta}$  (about 10%) is inferior to that of SNO+, the detection efficiency is much better (80%) due to its

double envelope.

The NEMO-3 experiment [67] combines calorimetry and tracking techniques. The foils of the source are surrounded by a tracking detector that provides a direct detection of the two electron tracks emitted in the decay. NEMO-3 is installed in the Frejus underground laboratory and is searching for neutrinoless double-beta decay for two main isotopes ( $^{100}\text{Mo}$  and  $^{82}\text{Se}$ ) and studying the two-neutrino double-beta decay of seven isotopes. The experiment has been taking data since 2003 and, up to the end of 2009, showed no evidence for neutrinoless double-beta decay.

SuperNEMO [68] uses the NEMO-3 approach with series of modules, each one consisting of a tracker and a calorimeter that surround a thin foil of the isotope. In SuperNEMO the target will likely be  $^{82}\text{Se}$ , although other isotopes such as  $^{150}\text{Nd}$  or  $^{48}\text{Ca}$  are also being considered. The mass of the target is limited to a few kilograms (typically 5–7 kg) by the need to build it foil-like, and to minimize multiple scattering and energy loss. The tracker and calorimeter can record the trajectory of the charged particles and measure their energies independently. This technique, which maximally exploits the topological signature of the events, leads to excellent background rejection. However, the selection efficiency is relatively low (about 30%), and the resolution rather modest (4% FWHM at  $Q_{\beta\beta}$ ). Moreover, this technique is very hard to extrapolate to large masses due to the size, complexity and cost of each module.

Another technique used in  $0\nu\beta\beta$  experiments is the xenon time projection chambers. Xenon is a suitable detection medium, providing both scintillation and ionization signals. It has a decaying isotope,  $^{136}\text{Xe}$ , with a natural abundance of about 10%. Compared to other sources, xenon is easy (thus relatively cheap) to enrich in the candidate isotope.

When an event occurs, the energetic electrons produced interact with the liquid xenon (LXe) to create scintillation light that is detected, for example, with avalanche photodiodes (APDs). The electrons also ionize some of the xenon and the ionized electrons drift to charge collection wires at the ends of the vessel in an electric field. The time between the light pulse and the electrons reaching the wires tell us how far in the event occurred, since we know the drift time.

There are two possibilities for a xenon TPC: a cryogenic liquid xenon time projection chamber (LXe TPC), or a (high-pressure) xenon (HPXe) gas chamber.

EXO [69] is a LXe TPC with a modest energy resolution (3.3% FWHM at  $Q_{\beta\beta}$ ) through ionization and scintillation readout. A 200 kg detector of 80% enriched  $^{136}\text{Xe}$  is currently being installed at the Waste Isolation Pilot Plant (WIPP) in New Mexico, USA. This experiment aims to measure the – as yet unobserved – two-neutrino mode of double-beta decay of  $^{136}\text{Xe}$  and provide a competitive limit on neutrinoless double-beta decay. Background rates of order 0.001 counts/keV kg yr are expected in EXO-200. The improvement with respect to the high-resolution calorimeters comes from the event topological information. The collaboration is undergoing extensive R&D to develop the xenon detector and a way to “tag” the products of the decay ( $^{136}\text{Ba}^{2+}$  tagging) in order to eliminate all backgrounds.

The NEXT experiment [70] proposes to build a 100 kg high-pressure gaseous xenon (enriched at 90% in  $^{136}\text{Xe}$ ) TPC. The experiment aims to take advantage of both good energy resolution ( $\leq 1\%$  FWHM at  $Q_{\beta\beta}$ ) and the presence of a  $0\nu\beta\beta$  topological signature for further background suppression. NEXT plans to rely on electroluminescence to amplify the ionization signal, using two separate photodetection schemes for an optimal measurement of both calorimetry and tracking.

Figure 37 shows the background rate in the region of interest (1 FWHM around  $Q_{\beta\beta}$ ) versus the energy resolution (FWHM) for different past and present experiments [71]. The (green) circles correspond to measured data, while the (blue) squares and (red) diamonds correspond, respectively, to the R (reference) and O (optimistic) background assumptions of the experiments, according to Ref. [71]. The results for the  $m_{\beta\beta}$  sensitivity (90% CL) of the proposals as a function of exposure are also shown. The filled circles indicate 10 years of run-time according to the reference scenario.

NEXT and CUORE have the best sensitivities, reaching 66 and 73 meV at 90% CL, respectively.

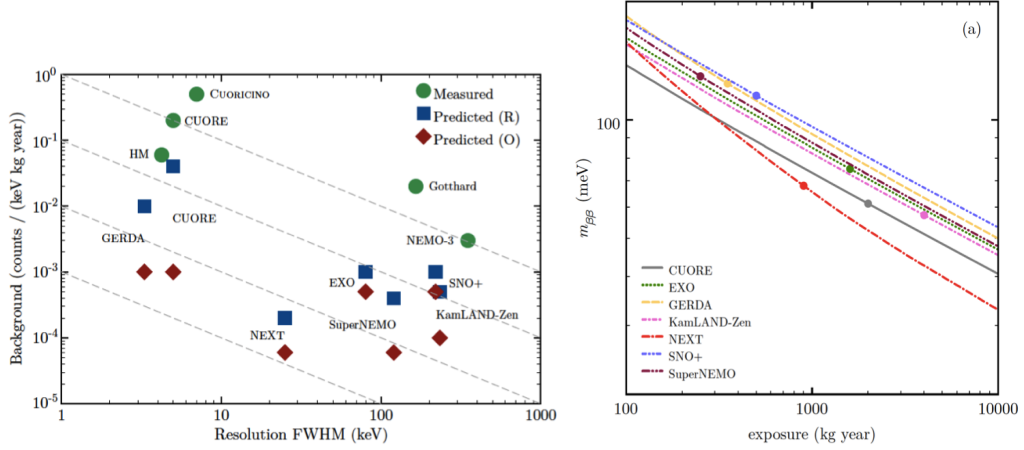


**Fig. 37:** (left) Background rate as a function of the energy resolution (FWHM) for different past and present experiments and (right)  $m_{\beta\beta}$  sensitivity (at 90% CL) as a function of the exposure (from Ref. [71]).

KamLAND-Zen, EXO and SuperNEMO follow, with sensitivities in the 82–87 meV range. GERDA and SNO+ reach sensitivities of 94 and 96 meV, respectively. In the optimistic scenario, the lower background regime for all experiments allows significantly better sensitivities to be obtained.

In summary, the goals of the next generation of  $0\nu\beta\beta$  experiments are to push the  $m_{\beta\beta}$  limit down to 100 meV to confirm or discard the Heidelberg–Moscow claim. In a second and more ambitious step, they should reach  $m_{\beta\beta} \sim 50$  meV to fully explore the degenerate spectrum. Finally, depending on their capability to scale their technology to larger masses ( $\sim$  ton scale), they will try to partially explore the inverse hierarchy down to  $\sim 10$  meV.

## 10 Supernova neutrinos

Type II supernovae (SNe) are massive stars that begin their lives made out of hydrogen. Hydrogen starts nuclear fusion in the core, and when all H is converted into He, the star starts to collapse until He is hot enough to fuse. Then, He will begin the same process as H. The same happens for the rest of the elements up to Fe. The Fe fusion reaction absorbs more energy than it releases, and then the core shrinks, heats up and produces no new, more massive elements. The star cannot resist the pressure of its internal gravitational force and then collapses. The collapse leads to an explosion, that is known as a type II SN.

In the core-collapse mechanism, three stages are important from the point of view of neutrino emission:

- (1) The collapse of the core: a first electron neutrino burst is emitted since the high density of matter enhances the electron capture by protons.
- (2) Then, neutrinos are trapped and an elastic bounce of the core is produced, which results in a shock wave. When the shock crosses the electron neutrino sphere, an intense burst of  $\nu_e$  is produced, called the *shock breakout* or *neutronization burst*, and a total energy of  $3 \times 10^{51}$  erg is radiated in milliseconds.
- (3) The process will finish in an explosion. Then, the external layers of the star are expelled into space. After this, the star loses energy by emitting neutrinos of all flavours and the *cooling process* ( $\sim 10$  s) starts until a neutron star or a black hole is formed.

The total energy released during this process is enormous:  $\approx 3 \times 10^{53}$  erg. Some 99% of the gravitational binding energy of the star ( $E_B$ ) is released in the form of neutrinos of all flavours: 1% are produced

during the neutronization process while the rest are  $\nu\bar{\nu}$  pairs from later cooling reactions. The expected supernovae rate in our Galaxy is about three per century.

In 1987 astrophysics entered a new era with the detection of the neutrinos from the SN1987A [72], which exploded in the Large Magellanic Cloud at a distance of  $\sim 50$  kpc. The burst of light was visible to the naked eye. Around three hours before the observation of the SN, an increase of neutrinos was detected by three water Cerenkov detectors: Kamiokande, IMB and Baksan. This observation confirmed important parts of the neutrino supernova theory such as total energy, mean temperature and time duration. However, limited quantitative information on the neutrino spectrum was obtained due to the small statistics (only about 20 events) recorded.

The flavour composition, energy spectrum and time structure of the neutrino burst from a supernova can give information about the explosion mechanism and the mechanisms of proto-neutron star cooling. In addition, the intrinsic properties of the neutrino such as flavour oscillations can also be studied.

The neutrinos in the cooling stage are in equilibrium with their surrounding matter density and their energy spectra can be described by a function close to a Fermi–Dirac distribution. The flux of an emitted neutrino  $\nu_\alpha$  can then be written as [73]

$$\phi_\alpha(E_\alpha, L_\alpha, D, T_\alpha, \eta_\alpha) = \frac{L_\alpha}{4\pi D^2 F_3(\eta_\alpha) T_\alpha^4} \frac{E_\alpha^2}{e^{E_\alpha/T_\alpha - \eta_\alpha} + 1}, \quad (51)$$

where  $L_\alpha$  is the luminosity of the flavour  $\nu_\alpha$  ( $E_B = \sum L_\alpha$ ),  $D$  is the distance to the supernova,  $E_\alpha$  is the energy of the  $\nu_\alpha$  neutrino,  $T_\alpha$  is the neutrino temperature inside the neutrinosphere and  $\eta_\alpha$  is the “pinching” factor.

The original  $\nu_\mu$ ,  $\nu_\tau$ ,  $\bar{\nu}_\mu$  and  $\bar{\nu}_\tau$  fluxes are approximately equal and therefore we treat them as  $\nu_x$ . An energy hierarchy between the different neutrino flavours is generally believed to hold and implies  $\langle E_{\nu_e} \rangle < \langle E_{\bar{\nu}_e} \rangle < \langle E_{\nu_x} \rangle$ . However, the specific neutrino spectra remain a matter of detailed calculations. In particular, recent simulations seem to indicate that the energy differences between flavours could be very small and possible collective neutrino flavour conversions could arise for either mass hierarchy depending on the primary fluxes [74].

Neutrino oscillations and matter effects in the supernova will change the neutrino fluxes significantly and, therefore, the number of events expected in the detectors.

If the neutrino energy spectra are different, then  $\theta_{13}$  and the mass hierarchy can be probed. For small mixing angle ( $\sin^2 \theta_{13} < 2 \times 10^{-6}$ ), there are no effects on  $\theta_{13}$  and we cannot distinguish among mass hierarchies. Only an upper bound on  $\sin^2 \theta_{13}$  can be set. For intermediate  $\theta_{13}$  ( $2 \times 10^{-6} < \sin^2 \theta_{13} < 3 \times 10^{-4}$ ), maximal sensitivity to the angle is achieved and measurements of the angle are possible in this region. For large mixing angle ( $\sin^2 \theta_{13} > 3 \times 10^{-4}$ ), maximal conversions occur. The mass hierarchy can be probed but only a lower bound on  $\theta_{13}$  can be established.

In addition to matter effects in the SN matter, when neutrinos traverse the Earth, regeneration effects can produce a distortion of the neutrino energy spectrum. If we compare the signals from different detectors in different locations, we could probe such an effect.

### 10.1 Supernova neutrino detection in terrestrial experiments

Most of the current and near-future supernova neutrino experiments [75] are water Cerenkov or liquid scintillator detectors and, therefore, primarily sensitive to the  $\bar{\nu}_e$  component of the signal, via inverse beta decay  $\bar{\nu}_e + p \rightarrow n + e^+$ . For supernova burst detection, not only statistics but also diversity of flavour sensitivity is needed: neutral current sensitivity, which gives access to the  $\nu_\mu$  and  $\nu_\tau$  components of the flux, and  $\nu_e$  sensitivity are particularly valuable.

Only two near-future experiments will be mainly sensitive to the  $\nu_e$ . The HALO detector [76] is under construction at SNOLab and it uses 80 tons of lead blocks instrumented with the unused SNO NCD

counters to record neutrons and electromagnetic signals. However, this technique has some limitations since no energy or pointing information can be obtained and only rates are provided. The ICARUS detector at Gran Sasso [77] is a 600 ton LAr TPC with excellent  $\nu_e$  sensitivity via  $^{40}\text{Ar}$  CC interactions, for which de-excitation gammas will be visible.

All current supernova neutrino experiments participate in the Supernova Early Warning System (SNEWS) [78], the network of SN neutrino observatories whose main goal is to provide the astronomical community with a prompt alert for the next galactic core-collapse supernova explosion.

Very promising for the future are a number of planned mega-detectors exploring essentially three technologies: megaton-scale water Cerenkov detectors, like LBNE in DUSEL [79], Hyper-K in Japan [80] and Memphys in Europe [81]; 100 kton-scale LAr TPC detectors, like GLACIER in Europe [82] or LAr LBNE in DUSEL [83]; and 50 kton-scale liquid scintillator detectors, like LENA in Europe [84] or Hanohano in Hawaii [85]. Some such detectors can hope to collect individual neutrino events every few years from beyond the Local Group of galaxies (a few megaparsecs), assuming that background can be reduced sufficiently.

The LAGUNA [86] project in Europe is studying the performance of these three technologies for detecting supernova neutrinos. The three proposed large-volume detector neutrino observatories can guarantee continuous exposure for several decades, so that a high statistics supernova neutrino signal could eventually be observed. The expected numbers of events for GLACIER, LENA and MEMPHYS are reported in Ref. [87], including the neutronization burst rates and diffuse supernova neutrino background.

## 10.2 Diffuse supernova neutrino background

The diffuse supernova neutrino background (DSNB) is the flux of neutrinos and antineutrinos emitted by all core-collapse supernovae that have occurred so far in the Universe. It will appear isotropic and time-independent in feasible observations. The DSNB has not been detected yet, but discovery prospects are excellent.

The Super-Kamiokande experiment established an upper limit on the  $\bar{\nu}_e$  flux of  $\Phi(\bar{\nu}_e) < 1.2 \text{ cm}^{-2} \text{ s}^{-1}$  for neutrino energies higher than 19.3 MeV [88], close to the predictions.

Figure 38 shows the energy spectrum of DSNB candidates. Points are data and the expected total atmospheric neutrino background is shown by the thick solid line. The largest allowed DSNB signal is shown by the shaded region added to the atmospheric background.

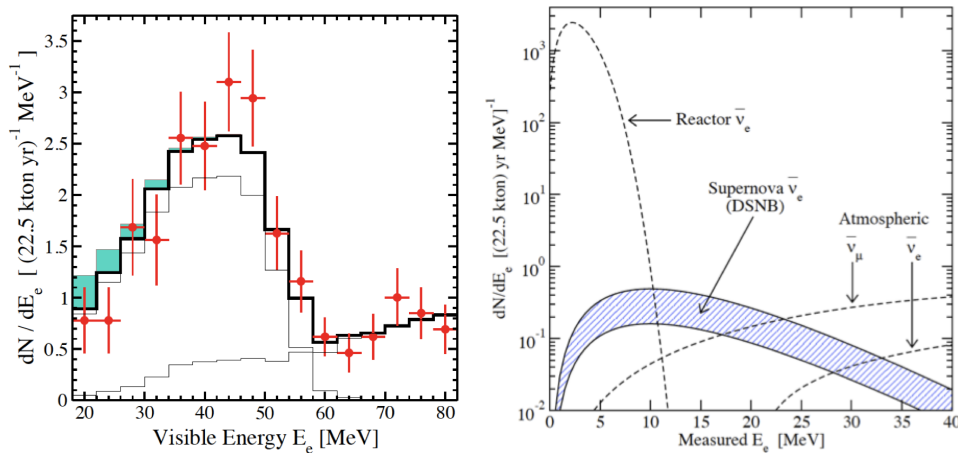


**Fig. 38:** (left) Energy spectrum of DSNB candidates measured by SK and (right) expected detection rates in SK with dissolved gadolinium (from Ref. [89]).

If Super-Kamiokande is modified with dissolved gadolinium to reduce detector backgrounds and increase the energy range for analysis, then the DSNB could be detected at a rate of a few events per year [89].

LAr TPCs would be able to detect mainly the  $\nu_e$  component of the DSNB signal, providing complementary information with respect to Super-Kamiokande. The main background sources for these events in the relevant neutrino energy range of 10–50 MeV are solar and low-energy atmospheric neutrinos. Depending on the theoretical predictions for the DSNB flux, a 100 kton LAr detector running for five years would get more than  $4\sigma$  measurement of the DSNB flux [90].

## 11 Conclusions

Neutrinos are responsible for one of the most important discoveries in the past few years in particle and astroparticle physics. Experimental data have proved that neutrinos oscillate and, therefore, they are massive particles.

Nevertheless, fundamental questions regarding neutrinos remain unsolved, and present and future neutrino experiments will try to provide an answer to them. The main goals of such a research programme include the measurement of the unknown  $\theta_{13}$  mixing angle, the sign of  $\Delta m_{32}^2$  (type of mass hierarchy), the determination of the existence or not of CP-violation in the leptonic sector, the value of the neutrino masses, and the Majorana or Dirac nature of neutrinos, among others. New facilities and detectors are being proposed to answer these questions, using both oscillation and non-oscillation experiments.

Neutrinos still have surprises for us, and the near future is going to be very exciting. We will have a better understanding of the neutrino physics thanks to the experimental programme in the coming years.

## Acknowledgements

I would like to thank the organizers for inviting me to this great School and in particular I am very grateful to the discussion leaders and students for creating a friendly environment and for very interesting discussions.

## References

- [1] C.L. Cowan, F. Reines, F.B. Harrison, E.C. Anderson and F.N. Hayes, *Science* **124** (1956) 103.
- [2] K. Nakamura *et al.*, *J. Phys.* **G37** (2010) 075021.
- [3] T. Kafka *et al.*, *Prog. Part. Nucl. Phys.* **64** (2010) 181–183.
- [4] P. Minkowski, *Phys. Lett.* **B67** (1977) 421.  
M.P. Gell-Mann, P. Ramond and R. Slansky, in *Supergravity*, Eds. P. van Nieuwenhuizen and D.Z. Freedman (North-Holland, Amsterdam, 1979).  
T. Yanagida, in *Proceedings of Workshop on Unified Theory and Baryon Number in the Universe*, Eds. O. Sawada and A. Sugamoto (KEK, Ibaraki, 1979).
- [5] L. Wolfenstein, *Phys. Rev.* **D17** (1978) 2369.  
S.P. Mikheev and A.Yu. Smirnov, *Yad. Fiz.* **42** (1985) 1441; *Nuovo Cim.* **9C** (1986) 17.
- [6] J.N. Bahcall and M.H. Pinsonneault, *Phys. Rev. Lett.* **92** (2004) 121301.
- [7] B.T. Cleveland *et al.*, *Astrophys. J.* **496** (1998) 505–526.
- [8] W. Hampel *et al.* (GALLEX Collaboration), *Phys. Lett.* **B447** (1999) 127–133.  
M. Altmann *et al.* (GNO Collaboration), *Phys. Lett.* **B616** (2005) 174–190.
- [9] J.N. Abdurashitov *et al.* (SAGE Collaboration), *Phys. Rev.* **C60** (1999) 055801.
- [10] Y. Fukuda *et al.* (Kamiokande Collaboration), *Phys. Rev. Lett.* **77** (1996) 1683.
- [11] S. Fukuda *et al.* (Super-Kamiokande Collaboration), *Phys. Rev. Lett.* **86** (2001) 5656–5660.

- [12] J. Boger *et al.* (SNO Collaboration), *Nucl. Instrum. Methods Phys. Res.* **A449** (2000) 172.
- [13] B. Aharmim *et al.* (SNO Collaboration), *Phys. Rev.* **C75** (2007) 045502.
- [14] B. Aharmim *et al.* (SNO Collaboration), *Phys. Rev. Lett.* **101** (2008) 111301.
- [15] B. Aharmim *et al.* (SNO Collaboration), *Phys. Rev.* **C81** (2010) 055504.
- [16] G. Alimonti *et al.* (Borexino Collaboration), *Nucl. Instrum. Methods Phys. Res.* **A600** (2009) 568.
- [17] C. Arpesella *et al.* (Borexino Collaboration), *Phys. Rev. Lett.* **101** (2008) 091302.
- [18] G. Bellini *et al.* (Borexino Collaboration), *Phys. Rev.* **D82** (2010) 033006.
- [19] T. Araki *et al.* (KamLAND Collaboration), *Nature* **436** (2005) 499–503.
- [20] G. Bellini *et al.* (Borexino Collaboration), *Phys. Rev.* **B687** (2010) 299–304.
- [21] Y. Fukuda *et al.* (Super-Kamiokande Collaboration), *Phys. Rev. Lett.* **81** (1998) 1562.
- [22] Y. Ashie *et al.* (Super-Kamiokande Collaboration), *Phys. Rev.* **D71** (2005) 112005.
- [23] Y. Ashie *et al.* (Super-Kamiokande Collaboration), *Phys. Rev. Lett.* **93** (2004) 101801.
- [24] R. Wendell *et al.* (Super-Kamiokande Collaboration), *Phys. Rev.* **D81** (2010) 092004.
- [25] M. Apollonio *et al.* (CHOOZ Collaboration), *Eur. Phys. J.* **C27** (2003) 331–374.
- [26] S. Abe *et al.* (KamLAND Collaboration), *Phys. Rev.* **C81** (2010) 025807.
- [27] K. Eguchi *et al.* (KamLAND Collaboration), *Phys. Rev. Lett.* **90** (2003) 021802.
- [28] T. Araki *et al.* (KamLAND Collaboration), *Phys. Rev. Lett.* **94** (2005) 081801.
- [29] A. Gando *et al.* (KamLAND Collaboration), *Phys. Rev.* **D83** (2011) 052002.
- [30] M.H. Ahn *et al.* (K2K Collaboration), *Phys. Rev.* **D74** (2006) 072003.
- [31] G.G. Michael *et al.* (MINOS Collaboration), *Nucl. Instrum. Methods Phys. Res.* **A596** (2008) 190.
- [32] P. Adamson *et al.* (MINOS Collaboration), *Phys. Rev. Lett.* **106** (2011) 181801.
- [33] P. Adamson *et al.* (MINOS Collaboration), *Phys. Rev. Lett.* **107** (2011) 021801.
- [34] P. Adamson *et al.* (MINOS Collaboration), *Phys. Rev.* **D82** (2010) 051102.
- [35] A. Aguilar *et al.* (LSND Collaboration), *Phys. Rev.* **D64** (2001) 112007.
- [36] B. Armbruster *et al.* (KARMEN Collaboration), *Phys. Rev.* **D65** (2002) 112001.
- [37] A.A. Aguilar-Arevalo *et al.* (MiniBooNE Collaboration), *Nucl. Instrum. Methods Phys. Res.* **A599** (2009) 28.
- [38] A.A. Aguilar-Arevalo *et al.* (MiniBooNE Collaboration), *Phys. Rev. Lett.* **98** (2007) 231801; *ibid.* **102** (2009) 101802.
- [39] A.A. Aguilar-Arevalo *et al.* (MiniBooNE Collaboration), *Phys. Rev. Lett.* **105** (2010) 181801.
- [40] K. Elsener (Ed.), *The CERN neutrino beam to Gran Sasso (Conceptual Technical Design)*, CERN 98-02, INFN/AE-98/05 (1998).  
R. Bailey *et al.*, *The CERN neutrino beam to Gran Sasso (NGS) (Addendum to report CERN 98-02, INFN/AE-98/05)*, CERN-SL/99-034(DI), INFN/AE-99/05 (1999).
- [41] N. Agafonova *et al.* (OPERA Collaboration), *Phys. Lett.* **B691** (2010) 138–145.
- [42] A. Menegolli *et al.* (ICARUS Collaboration), *J. Phys. Conf. Ser.* **203** (2010) 012107.
- [43] T. Schwetz *et al.*, *New J. Phys.* **13** (2011) 062004.
- [44] F. Ardellier *et al.* (Double Chooz Collaboration), arXiv:hep-ex/0606025.
- [45] J.K. Ahn *et al.* (RENO Collaboration), arXiv:hep-ex/1003.1391.
- [46] X. Guo *et al.* (Daya Bay Collaboration), arXiv:hep-ex/0701029.
- [47] K. Abe *et al.* (T2K Collaboration), *Nucl. Instrum. Meth.* **A659** (2011) 106.
- [48] K. Abe *et al.* (T2K Collaboration), *Phys. Rev. Lett.* **107** (2011) 041801.
- [49] D. Kielczewska *et al.* (T2K Collaboration), *Acta Phys. Polon.* **B41** (2010) 1565–1578.
- [50] D.S. Ayres *et al.* (NO $\nu$ A Collaboration), *The NO $\nu$ A Technical Design Report*, FERMILAB-

DESIGN-2007-01 (2007).

- [51] J. Bernabeu *et al.*, EURONU WP6 2009 yearly report: Update of the physics potential of Nufact, superbeams and betabeams [arXiv:1005.3146].
- [52] C. Kraus *et al.*, *Eur. Phys. J.* **C40** (2005) 447–468.  
V.N. Aseev *et al.*, *Phys. Rev.* **D84** (2011) 112003.
- [53] A. Monfardini *et al.*, *Nucl. Instrum. Methods Phys. Res.* **A559** (2006) 346–348.
- [54] A. Osipowiczka *et al.* (KATRIN Collaboration), arXiv:hep-ex/0109033.
- [55] B. Monreal and J.A. Formaggio, *Phys. Rev.* **D80** (2009) 051301.
- [56] L. Baudis *et al.*, *Phys. Rev. Lett.* **83** (1999) 41.  
C.E. Aalseth *et al.* (IGEX Collaboration), *Phys. Rev.* **D65** (2002) 092007.
- [57] H.V. Klapdor-Kleingrothaus *et al.*, *Mod. Phys. Lett.* **A16** (2001) 2409–2420.
- [58] H.V. Klapdor-Kleingrothaus *et al.*, *Phys. Lett.* **B586** (2004) 198–212.
- [59] H.V. Klapdor-Kleingrothaus *et al.*, *Mod. Phys. Lett.* **A21** (2006) 1547–1566.
- [60] G. Zuzel *et al.* (GERDA Collaboration), *Acta Phys. Polon.* **B41** (2010) 1469–1476.
- [61] V.E. Giuseppe *et al.* (Majorana Collaboration), *Nucl. Phys. (Proc. Suppl.)* **B217** (2011) 44–46.
- [62] T. Bloxham *et al.* (COBRA Collaboration), *Phys. Rev.* **C76** (2007) 025501.  
K. Zuber, *Phys. Lett.* **B519** (2001) 1.
- [63] E. Andreotti *et al.* (CUORICINO Collaboration), *Astropart. Phys.* **34** (2011) 822–831.  
C. Arnaboldi *et al.* (CUORICINO Collaboration), *Phys. Rev.* **C78** (2008) 035502.
- [64] F. Alessandria *et al.* (CUORE Collaboration), *Astropart. Phys.* submitted [arXiv:1109.0494].
- [65] C. Kraus *et al.* (SNO+ Collaboration), *Prog. Part. Nucl. Phys.* **64** (2010) 273–277.
- [66] A. Terashima *et al.* (KamLAND Collaboration), *J. Phys. Conf. Ser.* **120** (2008) 052029.  
M. Koga *et al.*, KamLAND double-beta decay experiment using  $^{136}\text{Xe}$ , Int. Conf. on High Energy Physics (ICHEP), Paris, July 2010.
- [67] M. Bongrand *et al.* (NEMO-3 Collaboration), arXiv:1105.2435.
- [68] C. Marquet *et al.* (SuperNEMO Collaboration), *Proc. Sci. PoS (ICHEP 2010)* 307.
- [69] C. Hall *et al.* (EXO Collaboration), *Proc. Sci. PoS (ICHEP 2010)* 300.
- [70] F. Grañena *et al.* (NEXT Collaboration), arXiv:0907.4054.
- [71] J.J. Gomez-Cadenas *et al.*, *J. Cosmol. Astropart. Phys.* **1106** (2011) 007.
- [72] K. Hirata *et al.*, *Phys. Rev. Lett.* **58** (1987) 1490.  
R. Bionta *et al.*, *Phys. Rev. Lett.* **58** (1987) 1494.  
E.N. Alekseev *et al.*, *JETP Lett.* **45** (1987) 589.
- [73] C. Lunardini and A.Y. Smirnov, *J. Cosmol. Astropart. Phys.* **0306** (2003) 009.
- [74] S. Choubey *et al.*, arXiv:1008.0308.
- [75] K. Scholberg, *J. Phys. Conf. Ser.* **203** (2010) 012079.
- [76] C.A. Duba *et al.*, *J. Phys. Conf. Ser.* **136** (2008) 042077.
- [77] I. Gil-Botella and A. Rubbia, *J. Cosmol. Astropart. Phys.* **0408** (2004) 001; *ibid.* **0310** (2003) 009.  
A. Bueno, I. Gil-Botella and A. Rubbia, arXiv:hep-ph/0307222.
- [78] P. Antonioli *et al.*, *New J. Phys.* **6** (2004) 114.
- [79] J. Maricic, *J. Phys. Conf. Ser.* **259** (2010) 012038.
- [80] K. Nakamura, *Int. J. Mod. Phys.* **A18** (2003) 4053.
- [81] A. Bellefon *et al.*, arXiv:hep-ex/0607026.
- [82] A. Rubbia, *J. Phys. Conf. Ser.* **171** (2009) 012020.
- [83] B. Baller *et al.*, LAr5 – A liquid argon neutrino detector for long baseline neutrino physics, FERMILAB-PROPOSAL-0982.



- [84] T. Marrodan Undagoitia *et al.*, *J. Phys. Conf. Ser.* **39** (2006) 278–280.
- [85] J. Maricic, *J. Phys. Conf. Ser.* **203** (2010) 012137.
- [86] A. Rubbia, *Acta Phys. Polon.* **B41** (2010) 1727–1732.
- [87] D. Autiero *et al.*, *J. Cosmol. Astropart. Phys.* **0711** (2007) 011.
- [88] M. Malek *et al.*, *Phys. Rev. Lett.* **90** (2003) 061101.
- [89] J.F. Beacom, *Annu. Rev. Nucl. Part. Sci.* **60** (2010) 439–462.
- [90] A.G. Cocco *et al.*, *J. Cosmol. Astropart. Phys.* **0412** (2004) 002.

## **Bibliography**

- C. Giunti and C.W. Kim, *Fundamentals of Neutrino Physics and Astrophysics* (Oxford University Press, Oxford, 2007).
- M.C. Gonzalez-Garcia and M. Maltoni, *Phenomenology with massive neutrinos*, *Phys. Rept.* **460** (2008) 1.
- K. Zuber, *Neutrino Physics*, Series in High Energy Physics, Cosmology and Gravitation, 2nd edn. (CRC Press, Boca Raton, FL, 2010).